Received: 27 November 2023 | Accepted: 12 July 2024

DOI: 10.1111/gcb.17462

Global Change Biology WILEY

RESEARCH ARTICLE

# Methane fluxes in tidal marshes of the conterminous United States

Ariane Arias-Ortiz[1,2] | Jaxine Wolfe[3] | Scott D. Bridgham[4] | Sara Knox[5,6] | Gavin McNicol[7] | Brian A. Needelman[8] | Julie Shahan[9] | Ellen J. Stuart-Haëntjens[10] | Lisamarie Windham-Myers[10] | Patty Y. Oikawa[11] | Dennis D. Baldocchi[2] | Joshua S. Caplan[12] | Margaret Capooci[13] | Kenneth M. Czapla[14] | R. Kyle Derby[15] | Heida L. Diefenderfer[16] | Inke Forbrich[17,18] | Gina Groseclose[19] | Jason K. Keller[20,21] | Cheryl Kelley[22] | Amr E. Keshta[23,24] | Helena S. Kleiner[3] | Ken W. Krauss[25] | Robert R. Lane[26] | Sarah Mack[27] | Serena Moseman-Valtierra[28] | Thomas J. Mozdzer[29] | Peter Mueller[30] | Scott C. Neubauer[31] | Genevieve Noyce[3] | Karina V. R. Schäfer[32] | Rebecca Sanders-DeMott[33] | Charles A. Schutte[34] | Rodrigo Vargas[13] | Nathaniel B. Weston[35] | Benjamin Wilson[36] | J. Patrick Megonigal[3] | James R. Holmquist[3]

**Correspondence**
Ariane Arias-Ortiz, Physics Department, Universitat Autònoma de Barcelona, Barcelona, Spain.
Email: ariane.arias@uab.cat

**Funding information**
Delta Stewardship Council, California, Grant/Award Number: 21034 and 49861; University Corporation for Atmospheric Research, Grant/Award Number: NA18NWS4620043B; National Aeronautics and Space Administration (NASA), Carbon Monitoring System:, Grant/Award Number: 80NSSC20K0084 and NNH20ZDA001N; Agencia Estatal de Investigación, Grant/Award Number: RYC2021-034455-I; Department of Energy, Grant/Award Number: COMPASS-FME and DE-AC05-76RL01830; National Science Foundation, Grant/Award Number: DEB-1655622

For affiliations refer to page 18.

## Abstract

Methane ($CH_4$) is a potent greenhouse gas (GHG) with atmospheric concentrations that have nearly tripled since pre-industrial times. Wetlands account for a large share of global $CH_4$ emissions, yet the magnitude and factors controlling $CH_4$ fluxes in tidal wetlands remain uncertain. We synthesized $CH_4$ flux data from 100 chamber and 9 eddy covariance (EC) sites across tidal marshes in the conterminous United States to assess controlling factors and improve predictions of $CH_4$ emissions. This effort included creating an open-source database of chamber-based GHG fluxes (https://doi.org/10.25573/serc.14227085). Annual fluxes across chamber and EC sites averaged $26 \pm 53$ g $CH_4$ $m^{-2}$ $year^{-1}$, with a median of 3.9 g $CH_4$ $m^{-2}$ $year^{-1}$, and only 25% of sites exceeding 18 g $CH_4$ $m^{-2}$ $year^{-1}$. The highest fluxes were observed at fresh-oligohaline sites with daily maximum temperature normals (MATmax) above 25.6°C. These were followed by frequently inundated low and mid-fresh-oligohaline marshes with MATmax ≤25.6°C, and mesohaline sites with MATmax >19°C. Quantile regressions of paired chamber $CH_4$ flux and porewater biogeochemistry revealed that the 90th percentile of fluxes fell below $5 \pm 3$ nmol $m^{-2}$ $s^{-1}$ at sulfate concentrations $>4.7 \pm 0.6$ mM, porewater salinity $>21 \pm 2$ psu, or surface water salinity $>15 \pm 3$ psu. Across sites, salinity was the dominant predictor of annual $CH_4$ fluxes, while within sites, temperature, gross primary productivity (GPP), and tidal height controlled variability at diel and seasonal scales. At the diel scale, GPP preceded temperature in importance for predicting $CH_4$ flux changes, while the opposite was observed at the seasonal scale. Water levels influenced the timing and pathway of diel $CH_4$ fluxes, with pulsed releases of stored $CH_4$ at low to rising tide. This study provides data and methods to improve tidal marsh $CH_4$ emission estimates, support blue carbon assessments, and refine national and global GHG inventories.

**KEYWORDS**
contiguous United States, eddy covariance, flux chamber, methane, open-source database, predictors, synthesis, tidal wetlands

## 1 | INTRODUCTION

Tidal wetlands play a critical role in global carbon (C) cycling (Bianchi, 2006; Odum, 2002). They have the potential to provide major feedbacks to the Earth's climate system as they exchange greenhouse gasses (GHGs) with the atmosphere, store large soil C pools, and have the potential to sequester C through continuous vertical accretion, allochthonous sediment deposition, and biomass accumulation (Duarte et al., 2013). Low rates of organic matter decomposition in their waterlogged soils promote the preservation of large quantities of soil organic C (also known as blue carbon) for centuries to millennia, contributing to the long-term removal of carbon dioxide ($CO_2$) from the atmosphere (Chmura et al., 2003).

However, the anaerobic conditions that promote soil C storage also lead to microbial methane ($CH_4$) production (Megonigal et al., 2004). Methane, with 32–45 times the warming potential of $CO_2$ over a 100-year time horizon, is second behind $CO_2$ in contributing to increases in atmospheric GHGs associated with recent warming (Forster et al., 2021; Neubauer & Megonigal, 2015). When considered in the timeframe relevant to meeting the Paris Agreement's target of limiting warming to 1.5°C, the $CH_4$ global warming potential is even higher, reaching 75 times that of $CO_2$ (Abernethy & Jackson, 2022). A recent compilation of global $CH_4$ emissions identified wetlands as among the primary natural sources of atmospheric $CH_4$, second only to freshwaters, with emissions ranging between 150 and 180 Tg $CH_4$ year$^{-1}$ (Saunois et al., 2020) and likely contributing to growing atmospheric $CH_4$ concentrations as the climate becomes warmer and wetter (Zhang et al., 2023), and anthropogenic wetland modifications increase (Kroeger et al., 2017; Rosentreter, Borges, et al., 2021). Global atmospheric $CH_4$ contributions from coastal wetlands, like tidal marshes, have been less studied (Rosentreter, Borges, et al., 2021), and recent bottom-up estimates (1–3.5 Tg $CH_4$ year$^{-1}$; Saunois et al., 2020) are not well constrained due to the lack of systematic observations, data quality (i.e., primarily discrete measurements with few high-frequency continuous measurements), uncertainties associated with coastal wetland area, and the risk of double counting of ecosystem types (e.g., tidal and non-tidal riverine, floodwater or estuarine wetlands) (Rosentreter et al., 2023; Rosentreter, Borges, et al., 2021; Roth et al., 2022; Saunois et al., 2020).

Global-scale controls on wetland $CH_4$ dynamics are reasonably known, including climatic zones, the presence of permafrost, peat, or mineral soils, groundwater, and surface water inputs in addition to precipitation, and the influence of salinity (Bridgham et al., 2013; Turetsky et al., 2014). These large spatial-scale characteristics subsequently control plant composition and the soil attributes that drive anaerobic C cycling and $CH_4$ dynamics. However, in tidal wetlands, where the tidal influence can dominate over other global factors, it remains unclear whether $CH_4$ responses to commonly studied predictors in non-tidal freshwater wetlands also apply. Tidal wetlands experience unique spatial and temporal variation in tides, redox conditions, and the influence of seawater (Cloern & Jassby, 2012; Seyfferth et al., 2020). These variations contribute to spatial gradients in plant species and traits, microbial communities, and processes such as soil accretion, primary production, respiration, and decomposition (Borde et al., 2020; Campbell & Kirchman, 2013; Morris et al., 2002; Watson & Byrne, 2009). Any or all of these factors substantially influence $CH_4$ emissions, highlighting the complexity of predicting $CH_4$ fluxes from these ecosystems.

On a local scale, rates of methanogenesis in wetland soils are primarily governed by the balance of electron donors and terminal electron acceptors. In general, saline tidal wetlands have high concentrations of porewater sulfate, typically leading to low rates of methanogenesis as acetate and hydrogen, primary substrates for methanogens, are utilized by sulfate reducers to decompose organic matter anaerobically (Megonigal et al., 2004). However, other pathways like methylotrophic methanogenesis can also be important in saline environments where non-competitive substrates are degraded to methyl compounds, producing $CH_4$ even when sulfate reduction co-occurs (Oremland et al., 1982; Seyfferth et al., 2020). Once $CH_4$ is produced, it can reach the atmosphere by physical (diffusion and ebullition) and plant-mediated processes. Some plants efficiently vent $CH_4$ to the atmosphere through aerenchymatous tissue. For example, in species such as *Phragmites australis*, *Typha latifolia, and T. angustifolia*, convective gas transport during light conditions allows $CH_4$ produced in soils to bypass $CH_4$ oxidation zones and escape to the atmosphere at greater rates (Bendix et al., 1994; Sanders-Demott et al., 2022; Van der Nat & Middelburg, 1998; Vroom et al., 2022).

Previous syntheses have identified important drivers of $CH_4$ emissions in tidal wetlands, including salinity and sulfate concentrations (Poffenbarger et al., 2011), temperature, and the quality and quantity of organic matter (Al-Haj & Fulweiler, 2020). Additionally, tidal pumping (Call et al., 2015; Trifunovic et al., 2020), dominant vegetation types and hydrology (Derby et al., 2022), plant phenological phases (Vázquez-Lule & Vargas, 2021), and functional trait composition (Mueller et al., 2020; Tong et al., 2018; Van der Nat & Middelburg, 1998) have been shown to play significant roles. While recent syntheses (Al-Haj & Fulweiler, 2020; Rosentreter, Al-Haj, et al., 2021; Rosentreter, Borges, et al., 2021) have qualitatively discussed these biogeochemical (e.g., salinity, temperature, organic matter) and biotic (e.g., plant-mediated transport) drivers, they have not resolved the relative influence of overlapping predictors in a quantitative fashion. This may be partly attributed to the reliance of syntheses on literature values, which often represent summarized flux averages or temporally upscaled estimates that can mask a wealth of processes and important variations evident in original disaggregated measurements. In contrast, this study focuses on original, disaggregated data and metadata obtained directly from researchers, allowing for a more detailed and in-depth analysis of $CH_4$ fluxes and their influencing factors.

Measuring $CH_4$ emissions from tidal marshes has primarily depended on chamber methods, especially static chambers sampled manually, due to their low cost, simplicity of application, and ease of deployment in areas without power (Rolston, 1986; Yu et al., 2013). The fine spatial resolution of chamber flux measurements, their generally low detection limits, and their compatibility with concurrent surface and porewater sampling of relevant analytes (salinity, pH, dissolved gas concentrations, or alternate electron acceptors) have made them an invaluable resource for process-based research and for measuring small fluxes and instances of net $CH_4$ oxidation. However, due to logistical constraints, chamber methods introduce limitations as they encourage sampling at low tide, during daylight hours, and on an intermittent sampling schedule (typically monthly). As a result, pulse events triggered by diurnal and tidal cycles, changes in atmospheric pressure, or sediment disturbances are often unobserved or filtered out to remove ebullition (Altor & Mitsch, 2006; Morin et al., 2014; Podgrajsek et al., 2014; Rosentreter et al., 2018).

To address the low resolution of daytime static chamber measurements, some studies have employed custom gas exchange models that incorporate continuous air temperature or water table depth, among other factors, to model $CH_4$ fluxes between sampling events (Krauss et al., 2016; Neubauer, 2013; Sanders-Demott et al., 2022; Schultz et al., 2023; Weston et al., 2014). In the absence of continuous measurements of predictor variables, others have used scaling factors to convert average daily fluxes into annual emissions (Bartlett & Harriss, 1993; Bridgham et al., 2006; Poffenbarger et al., 2011). These factors are based on studies that report both annual and daily rates and represent the ratio of annual $CH_4$ flux to average daily flux (Bridgham et al., 2006).

On the contrary, the continuous, high-frequency eddy covariance (EC) technique offers promising datasets for understanding tidal marsh $CH_4$ fluxes, which often involve nonlinear and asynchronous processes across multiple timescales (Reid et al., 2013; Sturtevant et al., 2016). However, EC studies in tidal marshes are less common than chamber studies and are not as widespread as in other ecosystems, such as inland freshwater wetlands, rice paddies, and tundra. Unlike chambers, EC systems are less effective in discerning the influence of factors operating at small spatial scales, such as plant traits and microtopography, and often lack supporting water level (Knox et al., 2019), salinity (Delwiche et al., 2021), and porewater data such as sulfate or nitrate concentrations that may pose important controls on $CH_4$ production. Nevertheless, they offer ecosystem-scale fluxes and are better suited for assessing the influence of plant C assimilation on $CH_4$ fluxes and pulsed events.

Drawing on data from both flux monitoring techniques increases the quantity of data available and leverages the benefits of both approaches to better understand the variability of $CH_4$ fluxes across time and space (Yuan et al., 2024). However, while EC data are available through global and national networks such as AmeriFlux and FLUXNET, chamber fluxes disaggregated by sampling event and supporting environmental covariates remain widely dispersed and frequently unavailable. In the context of the Coastal Carbon Network (CCN) Methane Working Group, we compiled, synthesized, and standardized chamber-based $CH_4$ fluxes across the conterminous United States (CONUS) and created an open-source database focused on tidal marsh ecosystems that host chamber-based GHG fluxes with supporting observations and porewater biogeochemistry (Arias-Ortiz et al., 2024).

Our primary objective was to assess controlling factors and improve predictions of $CH_4$ emissions in tidal marshes across CONUS. Here, we provide an in-depth analysis of tidal marsh $CH_4$ flux patterns and the factors influencing the variation in flux magnitudes and timing. Specifically, we address the following questions: (i) What are the primary predictors of $CH_4$ flux in tidal marshes across sites in CONUS? (ii) How does the variability in $CH_4$ fluxes change across daily to seasonal timescales, and what are the dominant predictors at each timescale? (iii) Can improved scaling factors for annualizing discrete chamber measurements be developed, and to what extent do daily and seasonal variations in $CH_4$ fluxes affect these factors? Finally, (iv) how can the identified relationships and gained information be used to improve monitoring and predictions of $CH_4$ emissions in tidal marshes?

## 2 | METHODS

### 2.1 | Dataset description

The database contains 35 contributed $CH_4$ flux datasets of 122 tidal marsh sites measured with chambers across CONUS (Arias-Ortiz et al., 2024). Details on the data acquisition process and database structure can be found in Supporting Information sections 1 and 2.

For the analysis in this study, we selected chamber plots without any experimental treatment, except for those involving salinity. These treatments consisted of slight changes from fresh to oligohaline conditions, resembling the seasonal variations in salinity that tidal marshes may naturally experience. This resulted in a total of 100 marsh sites with discrete $CH_4$ flux measurements disaggregated by sampling event, spanning from 1 day to 4 years, and accompanied by ancillary data, including porewater biogeochemistry. Analyses of the chamber dataset were complemented with nine independent EC tidal marsh datasets available through FLUXNET-$CH_4$ (US-LA1, US-LA2, US-Srr), AmeriFlux (US-EDN, US-Dmg, US-StJ), and tower-site PIs (US-MRM, US-HPY, and US-PLM) (Table S1), all of which adhere to standards and data QA/QC procedures explained elsewhere (Chu et al., 2023; Delwiche et al., 2021; Knox et al., 2019). Gap-filled fluxes were obtained from site PIs if missing in the original datasets. Likewise, when absent, water quality parameters, including conductivity or salinity and dissolved nitrate concentrations, were sourced from the USGS National Water Information System or National Estuarine Research Reserves online databases (NOAA, 2023; USGS NWIS 11180770, 2023). See Supporting Information section 1 and Table S1 for details on tower sites, including fraction of gap-filled $CH_4$ flux data.

Eddy covariance and chamber sites were classified using a multi-faceted classification system described in Table 1 and the Supporting Information section 2. The definition of "site" differs between chamber and EC studies. Eddy covariance sites are represented by the flux footprint rather than by gradients in biotic and abiotic factors such as elevation, species composition, or substrate type (channel, mudflat, or vegetated area). In this study, we defined chamber sites as distinct locations within a tidal wetland that could consist of several chamber plots. Adjacent areas, if composed of different wetland vegetation, salinity, elevation, or disturbance classes, were considered different chamber sites in our database.

### 2.1.1 | Chamber flux QA/QC and filtering

Submitted chamber-based $CH_4$ fluxes were assigned quality flags based on details reported during the data submission process or in the original publication (Table 2). These flags indicate if any thresholds ($R^2$ and/or $p$-value) were used to test, modify, or remove flux rates in the original studies. 65% of the submitted $CH_4$ fluxes were accompanied by $R^2$ and/or $p$-values (24% had both reported), and 35% had no associated statistics. Chamber flux measurements across studies in the synthesis varied in methodology. Some were based on syringe headspace samples, while others used continuous gas analyzers, which provide a more accurate assessment of concentration changes over time. To harmonize data quality control procedures across the dataset for analysis in this study, we filtered the data using percentiles (to remove outliers) and flux quality flags (Table 2). For the entire dataset, $CH_4$ fluxes below and above the 1st and 99th percentiles were excluded if statistics supporting these extreme values were not reported or if the $R^2$ of the regression was lower than 0.90 (Figure S2a). Furthermore, $CH_4$ flux rates flagged as "Not Significant" or "Not Tested" with reported statistics were further filtered out based on $p$-values, $R^2$, and the number of sample points ($n$) used to fit the regression model, all conditional on flux magnitude. Briefly, $CH_4$ flux rates with a $p$-value >0.10 were filtered out if they exceeded 10 nmol m$^{-2}$ s$^{-1}$ (the mean flux rate estimated for fluxes flagged as not significantly different from zero). If $p$-values were not provided but $R^2$ and $n$ were available, we filtered out fluxes exceeding 10 nmol m$^{-2}$ s$^{-1}$, those with $R^2 < 0.80$ and $n < 4$, or $R^2 < 0.55$ and $n < 6$. Rates <10 nmol m$^{-2}$ s$^{-1}$ were retained even if they did not meet the $R^2$ requirements because samples with low $CH_4$ concentrations generally have low $R^2$ values reflecting the low fluxes from those chambers rather than a poor measurement quality. Of 8980 individual chamber $CH_4$ fluxes, 156 were filtered out because they exceeded the 1st and 99th percentiles with no supporting statistics. An additional 60 measurements were discarded based on $p$, $R^2$, and $n$ values (Figure S2b). The result is a vetted dataset without unsubstantiated outliers of 8764 observations. We acknowledge that fluxes driven by nonlinear processes such as ebullition may be underrepresented.

## 2.2 | Annual $CH_4$ flux estimates and scaling factors

We estimated annual tidal marsh $CH_4$ fluxes where there was a full year of tower or chamber data. At EC sites, we calculated annual sums using gap-filled data. At chamber sites, we used published estimates where available. At sites where $CH_4$ fluxes had been measured across all months but annual estimates had not been reported, we integrated daytime fluxes using linear interpolation between year-round measurements after calculating the median of $CH_4$ flux rates within replicate chambers.

Most chamber sites (82 out of 100) did not have a full year of sampling coverage (i.e., one or more monthly measurements were missing). Additionally, two EC sites did not have a full year of data (US-PLM) or lacked gap-filled meteorological and flux variables (US-HPY). For these and the chamber sites lacking annual $CH_4$ flux measurements, we developed scaling factors to upscale measurements to annual estimates. Scaling factors were calculated from the ratio between annual flux (in units of g $CH_4$ m$^{-2}$ year$^{-1}$) and average daily flux (in mg $CH_4$ m$^{-2}$ day$^{-1}$) using sites with a full year of sampling coverage (Bridgham et al., 2006). Scaling factors were calculated for both chamber and EC sites. At EC sites, we used non-gap-filled mean daily flux measurements against the annual sum calculated with gap-filled data. If a specific site-year had more than 2 consecutive months of missing data, we excluded it from the computation of scaling factors.

Particularly, we were interested in developing a scaling factor specific to the peak emission period (annual flux/average daily flux between June and August) since chamber studies in temperate marshes do not often include winter sampling when plant productivity is at its lowest (e.g., Bartlett, 1985; Weston et al., 2014) and most sites in the database met the condition of having data

**TABLE 1** Attribute categories used to classify chamber and EC sites in according to wetland type, vegetation, salinity, relative elevation, and disturbance conditions.

| Attribute | Code | Description |
|---|---|---|
| Wetland type | Palustrine tidal | Wetlands dominated by trees, shrubs, or emergents that occur in tidal areas where salinity is <0.5 psu (Cowardin et al., 1979) |
| | Estuarine intertidal | Tidal wetlands usually semi-enclosed by land but have open, partly obstructed, or sporadic access to the open ocean, and in which ocean water is diluted by freshwater runoff from the land. Salinities >0.5 psu (Cowardin et al., 1979) |
| Vegetation Class | Mudflat | Describes unvegetated areas exposed and flooded by tides |
| | Emergent | Describes wetlands dominated by persistent emergent vascular plants |
| | Scrub/Shrub | Describes wetlands dominated by woody vegetation ≤5 m in height |
| | Forested | Describes wetlands dominated by woody vegetation >5 m in height |
| Salinity class | Fresh | <0.5 psu |
| | Oligohaline | 0.5–5 psu |
| | Mesohaline | 5–18 psu |
| | Polyhaline | 18–30 psu |
| | Mixoeuhaline | 30–40 psu |
| Elevation Class | High | Elevation above the Mean Highwater mark (MHW), inundated infrequently. Could be defined by vegetation communities (e.g., *Spartina patens*, *Distichlis spicata*, *Salicornia* sp., *Juncus* sp., and bulrush species) |
| | Mid | Elevation in the relative middle of the tidal frame, frequently inundated, typically defined by vegetation communities (e.g., *Spartina patens*) |
| | Low | Elevation relatively low in the tidal frame, frequently inundated, typically defined by vegetation communities (e.g., *Spartina alterniflora*) |
| | Levee | Study-specific definition of a relatively high elevation zone built up on the edge of a river, creek, or channel |
| | Back | Study-specific definition of a relatively low elevation zone behind a levee |
| Disturbance class | Undisturbed | No disturbance or management has occurred on the site |
| | Tidally restored | Tidal flow has been restored by removing an artificial obstruction |
| | Tidally restricted | Tidal flow is muted or blocked by built structures. Includes impoundment |
| | Ditched | Tidal hydrology is altered because artificial ditches have been cut to promote tidal flooding and drainage |
| | Species invasion | Establishment of non-native species that compete with, displace, or even eliminate native species |
| | Submergence-Salinization | Caused by sea level rise and saltwater intrusion |
| | Storm disturbance | Major storms, including unusually high precipitation and/or wind events |
| | Removal of invasive plants | Natural plant communities have been restored by actively removing invasive plant species |
| | Revegetation | Wetland vegetation has been reintroduced by replanting on unvegetated surfaces |
| | Wetland construction | Constructed wetland using sediments such as dredge spoils or other sediment source |

during this period. For sites lacking annual $CH_4$ flux measurements, we provided a first-order estimation of their annual $CH_4$ flux using the scaling factor derived from June–August mean daily $CH_4$ fluxes (without gap-filling for EC sites). We refrained from scaling mean daily $CH_4$ fluxes to annual estimates at chamber sites with a study duration ≤1 day (sites = 4). We averaged annual fluxes when there was more than 1 year of data for a given chamber or EC site. Additionally, we added two sites for which disaggregated data could not be synthesized (i.e., not in the dataset) but measured annual $CH_4$ fluxes had been published (Neubauer et al., 2000; Segarra et al., 2013).

We treated annual $CH_4$ flux estimates from chambers and EC as comparable, making no distinction between the two when estimating mean, median, and geometric mean annual $CH_4$ fluxes across tidal marshes in the CONUS. Previous synthesis works have also combined chamber and EC annual $CH_4$ flux estimates due to the limited number of EC sites in tidal or coastal settings compared with those of chambers (Al-Haj & Fulweiler, 2020; Rosentreter et al., 2023).

**TABLE 2** Flagging criteria for chamber $CH_4$ flux analysis based on their statistical significance and treatment in original studies.

| Flag | Description |
|---|---|
| "Not Tested" (NT) | Assigned to flux rates missing statistics or any flux not censored or modified based on $R^2$ or *P*-values, even if these were provided in the original publication |
| "Not Significant" (NS) | Assigned to flux rates considered not significantly different from zero by the authors, divided into two subcategories<br>NS_0: Used when authors replaced non-significant flux rates with zero<br>NS_NA: Assigned when authors removed non-significant flux rates at specific sampling events |
| "Significant" (S) | Assigned to all flux rates accompanied by linear regression statistics and considered significantly different from zero by authors, regardless of study-specific thresholds |

Scaling factors and $CH_4$ flux data had non-normal distributions; thus, we focused on comparing medians and used non-parametric tests such as paired-sample Signed test (S) for paired comparisons (i.e., year-round vs. June–August scaling factors), Mann–Whitney test (U) for two-group comparisons (e.g., scaling factors between EC and chambers), or a Kruskal–Wallis Dunn's test (H) using the Benjamini–Hochberg correction for multiple comparisons (i.e., fluxes between salinity, elevation, and disturbance classes). All statistical analyses were done at a level of significance of $\alpha < 0.05$.

## 2.3 | Analysis of predictors of $CH_4$ fluxes across sites

### 2.3.1 | Predictors of annual $CH_4$ fluxes using broadly available data

To evaluate the predictors of annual $CH_4$ fluxes across sites in CONUS, we combined chamber and EC annual $CH_4$ flux estimates and used qualitative (e.g., salinity and elevation class) and long-term climatological data (i.e., climate normals), which were broadly available at all sites. These data were fit to classification and regression trees such as Conditional Inference Trees (CTree) (Hothorn et al., 2006) and Random Forests (RF) (Breiman, 2001). CTrees use a significance test procedure to select variables at each split to reduce overfitting and selection bias. The stopping criterion is implemented when the global null hypothesis of independence between the response and any of the covariates cannot be rejected at a nominal level α, set at 0.05. The tree was constructed using the function "ctree" in the R package "Partykit" (Hothorn & Zeileis, 2015), limiting the tree depth to five levels. CTrees provide direct visualization of the splits at decision nodes, helping the interpretability of predictors, and are similar to binary partitioning methods used for analyzing soil $CO_2$ efflux measurements in terrestrial ecosystems (Vargas et al., 2010). However, they may suffer from issues associated with single trees, such as overfitting, high variance, or bias toward dominant classes.

For this reason, we added RF to our analysis. We trained a RF algorithm for annual $CH_4$ fluxes using R's "caret" package (Kuhn, 2008). Similar to CTrees, the RF model was trained on all available data (i.e., we did not create training and test data splits) since our objective was to determine the hierarchy of predictor importance of $CH_4$ fluxes in tidal wetlands rather than to identify a predictive model that can generalize to new conditions (Knox et al., 2021). Hyperparameter tuning was performed for mtry (number of predictors randomly sampled at each decision node, selected at 6), and the number of trees was set to 400. For CTrees and RF models, we provide out-of-bag model fit metrics (coefficient of determination, mean absolute error, and root mean squared error) to further evaluate relative confidence in results.

Long-term average normals included in CTree and RF analyses were mean annual temperature and precipitation (MAT and MAP), mean daily maximum annual temperature and vapor pressure deficit (MATmax and VPDmax), and mean total daily shortwave solar radiation (Soltotal), which were extracted from PRISM using specific site coordinates (PRISM Climate Group, Oregon State University, https://prism.oregonstate.edu, data generated November 10, 2022). For these analyses, back and levee elevation classes (Table 1) were grouped within the low and high elevation classes, respectively, due to their low representation (less than three sites each) across the dataset. Salinity class was converted to numeric format to run the RF algorithm. Mean annual surface water or porewater salinity was calculated at sites with available data, while the midpoint of the salinity class range was used at sites with no salinity data.

### 2.3.2 | Predictors of $CH_4$ fluxes using discrete chamber measurements

To evaluate predictors of $CH_4$ flux across sites using chamber-disaggregated $CH_4$ fluxes by sampling event and time-specific environmental parameters, we employed generalized additive models (GAMs) (Hastie & Tibshirani, 1990). We chose GAMs over regression trees like RF because we prioritized interpretability over predictive performance. Additionally, discrete chamber data present challenges due to patchiness in recorded variables, highlighting a lack of standardization across chamber studies and, consequently, the need for developing models for each recorded variable individually when using the entire dataset. GAMs can describe linear and nonlinear relationships between $CH_4$ fluxes and predictor variables, and they have the advantage of not needing data transformation. Before running GAMs and any of the following analyses, we transformed periodic variables such as day of year (DOY) and sample hour using their sine and cosine transformations instead of their original values to linearize their cyclical pattern. First, we developed GAMs of $CH_4$ flux using each predictor individually. Relative predictor importance was determined by comparing the deviance explained among predictors. From the entire database, we selected predictors that were available in five or more studies. Then multivariate GAMs were implemented using a combination of predictors that individually explained the largest variance and were present in at least five studies. Models were fit with restricted maximum likelihood (REML), and study ID (i.e., publication) was included as a random factor to account for non-independence of multiple chamber fluxes extracted from the same study. Additionally, the presence or absence of flux $R^2$ or $p$-values was used as an estimate of precision and was applied to weight flux rates so that studies in which statistics had supported $CH_4$ fluxes were given a higher weight (0.8 vs. 0.2). All GAMs were implemented using the R "*mgcv*" package (Wood, 2011).

Leveraging nonlinear quantile regression, we established quantitative relationships between $CH_4$ emissions and the top-ranked predictor variables identified by GAMs, and estimated thresholds above which $CH_4$ fluxes were negligible. Quantile regression is valuable when assumptions like normality are not met. Additionally, this approach is adept at resisting the influence of outliers and is well suited for handling heteroscedasticity (i.e., where the variance of the $CH_4$ fluxes varies across different levels of a predictor, e.g., salinity) (Koenker, 2005). It allows for more accurate modeling of the varying spread of $CH_4$ fluxes by estimating multiple slopes that describe the relationships between specific quantiles of the $CH_4$ flux distribution and a predictor that regression methods, focused solely on predicting mean values, would otherwise overlook (Cade & Noon, 2003). Quantile regressions were fitted for the 0.1, 0.5, and 0.9 quantiles of $CH_4$ fluxes using the nlrq() function within the R package *"quantreg"* (Koenker, 2023) due to the observed nonlinear relationships between $CH_4$ fluxes and the tested predictor variables. The slopes of the fitted conditional quantile regressions were used to estimate the predictor level required to decrease $CH_4$ fluxes by half, based on an exponential decay relationship (i.e., $X_{1/2} = \ln(2)/\text{slope}$). Subsequently, threshold values were estimated as seven times $X_{1/2}$, representing a 99% reduction of $CH_4$ fluxes through interactions with increasing predictor levels. We calculated these thresholds for the 50th and 90th percentiles of the conditional distribution of $CH_4$ fluxes, representing the predictor thresholds below which the 50% and 90% of the highest $CH_4$ fluxes occur, respectively.

## 2.4 | Analysis of predictors of $CH_4$ fluxes across timescales

Half-hourly EC datasets were used to assess $CH_4$ flux magnitude fluctuations at diel to seasonal scales and their controlling factors. Additionally, they provided insights into the significance of predictor variables not often evaluated in chamber studies, such as plant activity through GPP, net ecosystem exchange, or latent heat, as well as the effects of tidal pulsing on modulating $CH_4$ exchange.

We employed wavelet time series decomposition to identify major timescales of variation within the continuous $CH_4$ flux time series. Then, we used mutual information ($I$) to find the relative importance of each predictor variable and identify both synchronous and asynchronous interactions (Ruddell et al., 2013). Mutual information ($I$) measures the amount of information shared by two variables, $X$ and $Y$, or the reduction in uncertainty of one variable given the knowledge of the other variable (Fraser & Swinney, 1986). The degree of mutual information between $X$ and $Y$ is increased by adding a time lag (positive or negative) in series $Y$ relative to $X$, thereby allowing the identification of both synchronous and asynchronous interactions. Using the ProcessNetwork Software (v1.5, Ruddell et al., 2008) and the Wavelet Methods for Time Series Analysis (WMTSA) toolkit (Cornish et al., 2003), we decomposed gap-filled $CH_4$ flux and explanatory variables in four general timescales of variation: hourly (1–2 h), diel (4 h–1.3 days), multiday (2.7–21.3 days), and seasonal (42.7–341 days). These timescales of variation represented short-term perturbations such as wind gusts or overpassing clouds, day-night changes in meteorological variables and tidal fluctuations, neap-spring tidal cycles, and seasonal courses of solar movement and vegetation phenology, respectively. Wavelet decomposition was performed on gap-filled, half-hourly data using the maximal overlap discrete wavelet transform (MODWT), summing the detail over adjacent scales to yield the latter four timescales of variation (details in Sturtevant et al., 2016). Wavelet decomposed data were then used to compute the mutual information between $CH_4$ fluxes and biophysical variables within each timescale over a range of time lags (from half a day at the diel scale to 60 days at the seasonal scale). Original gaps in the reconstructed time series were reintroduced before mutual information calculation for all except the seasonal analysis following (Knox et al., 2021). Results were interpreted using the relative mutual information ($I^R$) metric, a normalized measure of the statistical dependence of $CH_4$ flux on a range of predictor variables, with larger values indicating higher dependence. To determine the relative importance of each predictor variable, we ranked the normalized $I^R$ values across sites, and we did that within each timescale of interest. In this study, we followed the methods described by Knox et al. (2021) (i.e., 10 bins and 50 random reshufflings to calculate significance thresholds at each lag) and focused on results for the predictors of diel, multiday, and seasonal timescales. The hourly wavelet scale is often dominated by noise (Hollinger & Richardson, 2005) and was only produced to show the distribution of $CH_4$ flux variability across timescales.

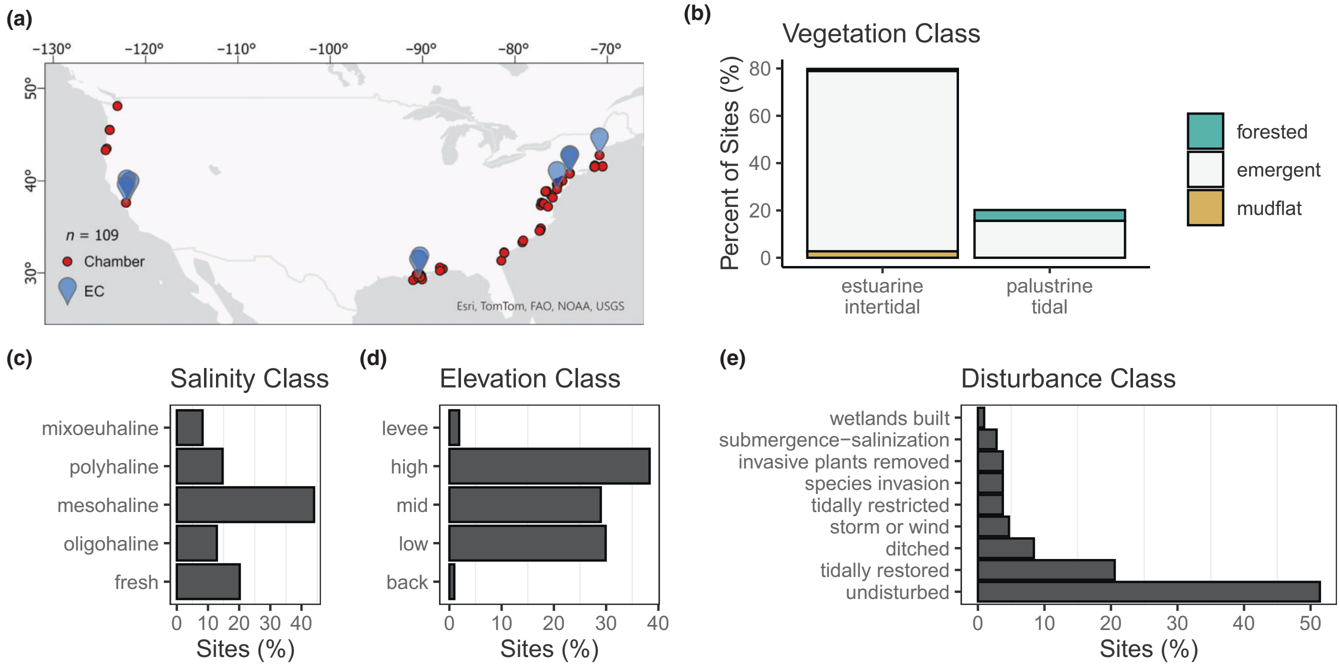


**FIGURE 1** Location of sites included in this synthesis (a) and characteristics of $CH_4$ flux rates contained in the database. Sites are classified based on wetland vegetation type (b), salinity (c), elevation (d), and disturbance (e).

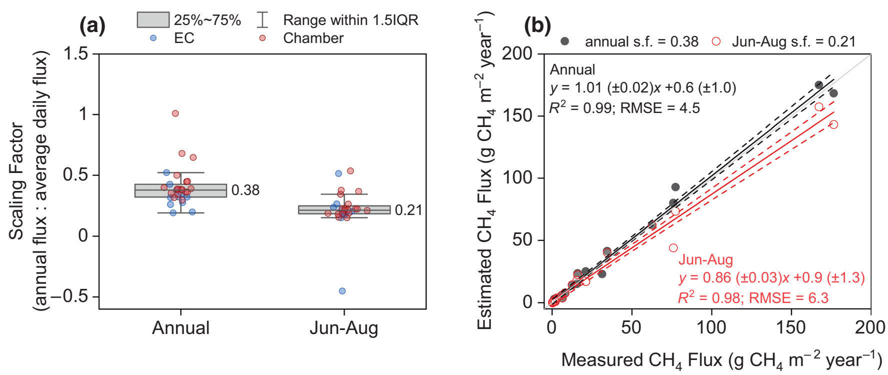


**FIGURE 2** Annual $CH_4$ flux scaling factors. Scaling factors estimated using average daily fluxes over the course of a year and from June to August (a). Relationship between measured and estimated annual $CH_4$ flux using the annual (solid circles) or the June–August scaling factor (open circles) (b). Linear regression fits show 95% confidence bands. Results in panels (a) and (b) include EC and chamber datasets with a year of sampling coverage.

## 3 | RESULTS

The final database contained 44 contributed datasets with 109 (100 chamber and 9 EC) tidal marsh sites, with measurements from 1980 to 2022. The dataset was dominated by $CH_4$ fluxes from tidal mesohaline wetlands with emergent vegetation, predominantly located on the US East Coast (Figure 1). Similar proportions (~30%–40%) of high, mid, and low tidal marsh environments were represented, with fewer sites located in environments affected by banks, berms, or levees. Half of the sites corresponded to undisturbed tidal marshes, followed by tidally restored (20%), ditched (8%), and other disturbance classes with a minority representation (<5%), including tidally restricted sites and species invasion (4%). Chamber-based data were unequally distributed throughout the year, with more observations concentrated from June to August (Figure S3). Five of the nine EC tower sites had paired chamber $CH_4$ flux measurements. Carbon dioxide and $N_2O$ fluxes were also compiled alongside $CH_4$ and are available in 52% and 30% of the sites, respectively, but they were not the focus of this synthesis.

### 3.1 | Scaling factors

A total of 29 site-years (11 from EC, 18 from chambers) had data covering all months of the year; hence, they were used to compute annual $CH_4$ flux scaling factors. Median scaling factors (s.f.) differed significantly when calculated based on daily fluxes averaged year-round (0.38, IQR = 0.10) compared to when considering

June–August daily average fluxes (0.21, IQR = 0.06) ($S = 3$, $z = 3.97$, $P < 0.001$) (Figure 2a). Scaling factors estimated using year-round daily averages were significantly lower for EC (s.f. = 0.32) than for chamber measurements (s.f. = 0.39) ($U(N_{EC} = 11, N_{chamber} = 18) = 42$, $z = -2.54$, $p = .01$), but no significant differences in the scaling factor were observed between methods when using daily averages from June to August ($U(N_{EC} = 10, N_{chamber} = 18) = 69$, $z = -0.98$, $p = .33$). For the 29 site-years (EC and chamber combined), the annual $CH_4$ fluxes estimated using the June–August scaling factor closely agreed with the measured values (Figure 2b). We did not find significant differences in annual scaling factors between wetland types ($U(N_{estuarine\ intertidal} = 23, N_{palustrine\ tidal} = 5) = 53$, $z = -0.24$, $p = .81$), salinity classes ($H(4) = 2.0$, $p = .74$), elevation classes ($H(4) = 2.8$, $p = .60$), or disturbance classes ($H(4) = 4.8$, $p = .30$) (Tables S2–S5).

## 3.2 | Tidal Marsh annual $CH_4$ flux estimates

Using available full site-year data, published fluxes, and scaling factors at sites where the sampling coverage was shorter than a year, we estimated annual $CH_4$ fluxes from tidal marshes in CONUS. From a total of 108 sites including chamber and EC datasets, mean ± SD annual $CH_4$ fluxes were 26 ± 53 g $CH_4$ $m^{-2}$ $year^{-1}$, but the central tendency of the estimates represented by the median and the geometric mean were seven to five times lower, at 3.9 and 5.4 g $CH_4$ $m^{-2}$ $year^{-1}$, respectively (note that the geometric mean excludes sites with negative or zero annual $CH_4$ fluxes) (Figure 3a). Median $CH_4$ fluxes were significantly higher at freshwater sites than at mesohaline, polyhaline, and mixoeuhaline marshes ($H(4) = 28.06$, $p < .001$) (Figure 3b). Statistical overlap of annual $CH_4$ fluxes existed between fresh and oligohaline, oligohaline and mesohaline, and polyhaline and mixoeuhaline conditions. However, when using chamber flux data disaggregated by sampling event, differences between salinity classes were more pronounced, with only fresh and oligohaline conditions showing statistical overlap ($z = -1.93$, $p = .27$) (Figure 3c). The variance of $CH_4$ fluxes at fresh and oligohaline sites was 27, 700, and >5000 times larger than at mesohaline, polyhaline, and mixoeuhaline sites, respectively. No statistical differences were observed between the distributions of chamber- and EC-derived annual fluxes across CONUS or when aggregated by salinity class (Table S6).

The wide numerical range and the right-skewed nature of the $CH_4$ flux data were also observed in annual $CH_4$ fluxes when separated by salinity class, which additionally showed a slight bimodal distribution (Figure S4). In fresh-oligohaline and mesohaline conditions, there was a trend of higher $CH_4$ fluxes in low than high marsh environments, but this pattern was not observed in more saline sites (Figure S5). The assessment of disparities in $CH_4$ flux between disturbance classes was limited due to the uneven distribution of sites across salinity classes. When sites were grouped by salinity, tidally restored mesohaline marshes exhibited significantly lower $CH_4$ fluxes than *Phragmites*-invaded sites (Figure S5). Upon exploring chamber $CH_4$ fluxes disaggregated by sampling event grouped by salinity and species, chambers featuring *Phragmites* exhibited higher $CH_4$ fluxes than those where other species were present (Figure S6). This trend was only notable in mesohaline and polyhaline marshes, where most data were available. However, the generalizability of these results to $CH_4$ fluxes from other salinity classes could not be assessed due to the incomplete representation of disturbance classes in non-mesohaline salinity conditions.

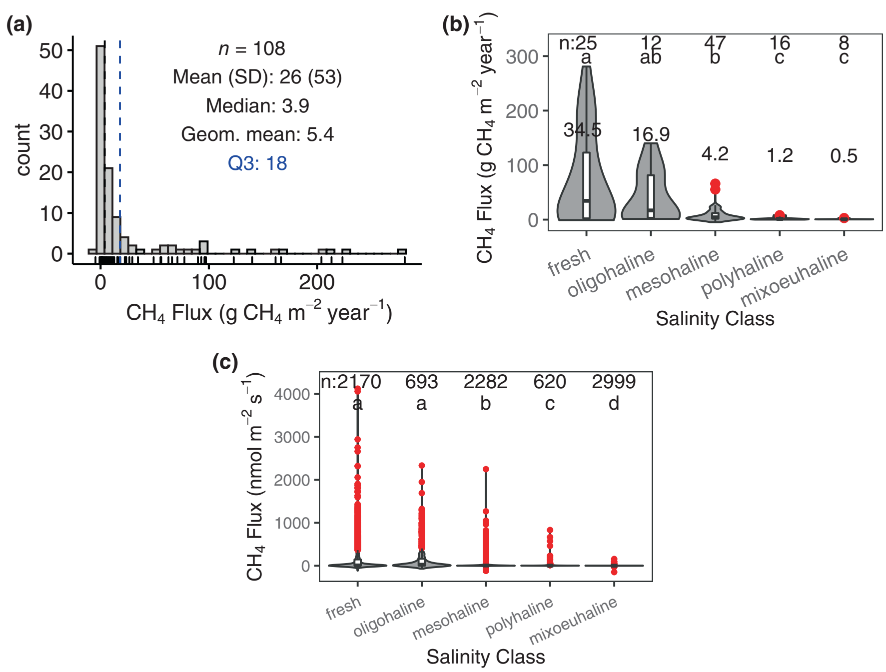


FIGURE 3 Tidal marsh $CH_4$ fluxes. Histogram of annual $CH_4$ fluxes (a), annual $CH_4$ fluxes grouped by salinity class (b), and chamber-based $CH_4$ fluxes disaggregated by sampling event grouped by salinity class (c). Panel (a) and (b) combine results from chamber and eddy covariance sites. On panel a, vertical lines (or rug) across the *x*-axis project individual data points and their distribution. On panels b and c, red dots indicate outliers and different lower-case letters represent significant differences between salinity classes as a result of a Kruskal–Wallis Dunn's multiple comparison test with $p < .05$ adjusted using the Benjamini–Hochberg procedure ($p < \alpha/2$). Values on the box plot in panel (b) represent median annual $CH_4$ fluxes at each salinity class.

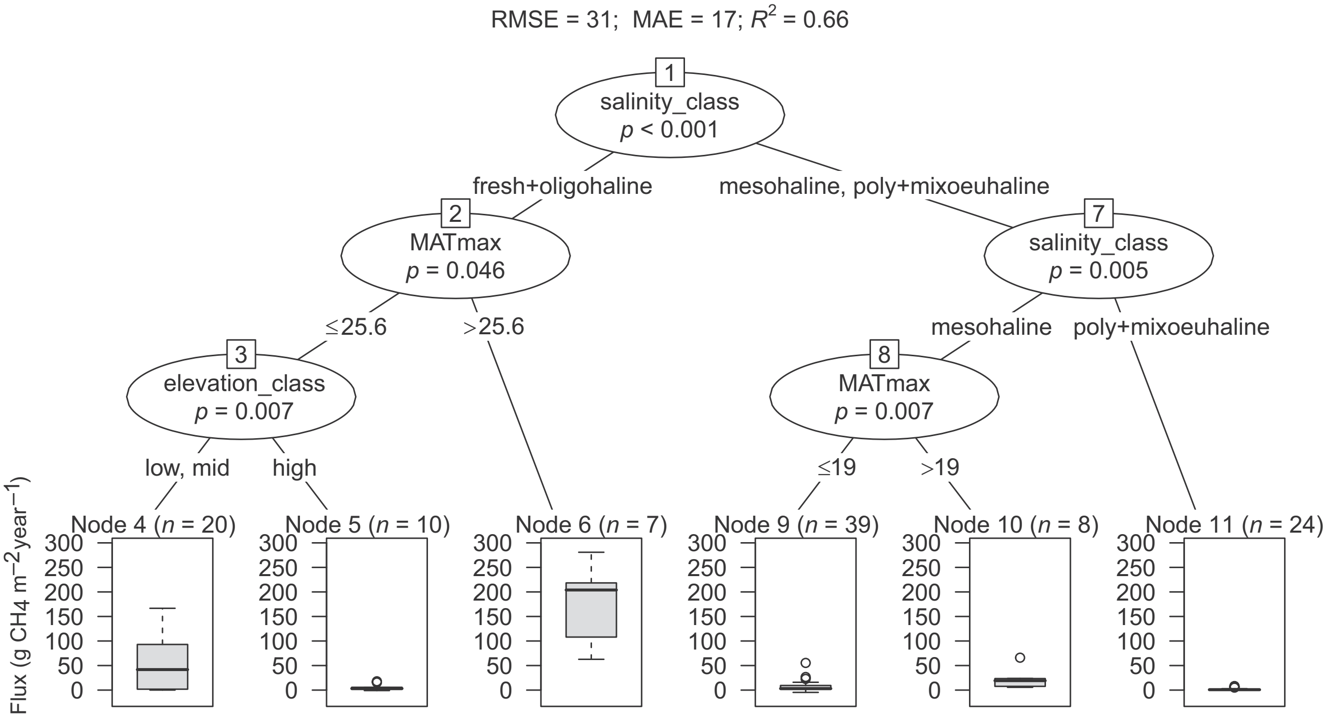


**FIGURE 4** Conditional inference tree based on salinity class (with fresh and oligohaline, and polyhaline and mixoeuhaline classes combined), long-term mean daily maximum annual temperature (MATmax) and elevation class. MATmax represents the "normal" or average maximum temperature for each day of the year based on 30-year historical data. Box plots show annual $CH_4$ flux in g $CH_4$ $m^{-2}$ $year^{-1}$. Results of the CTree include eddy covariance and chamber data.

## 3.3 | Predictors of $CH_4$ flux across sites

### 3.3.1 | Predictors of annual $CH_4$ flux

Results of both the CTree and RF methods were similar, ranking salinity as the most important predictor of the magnitude of annual $CH_4$ fluxes, followed by mean daily maximum annual temperature (MATmax) and, to a minor extent, elevation class and mean daily maximum annual vapor pressure deficit (Figure 4; Figure S7). These rankings were obtained using EC and chamber-based annual estimates combined. Average model performance was highest for RF with an out-of-bag $R^2$ of 0.94, MAE (mean absolute error) of 7.9 g $CH_4$ $m^{-2}$ $year^{-1}$, and RMSE of 14 g $CH_4$ $m^{-2}$ $year^{-1}$ (Figure S7). The best resulting CTree ($R^2$ = 0.66, MAE = 17, RMSE = 31 g $CH_4$ $m^{-2}$ $year^{-1}$) was achieved when fresh and oligohaline, and polyhaline and mixoeuhaline classes were combined. This CTree was composed of 11 decision nodes, with salinity at the root of the tree, followed by MATmax and elevation class. The highest annual $CH_4$ fluxes were observed at fresh and oligohaline sites with MATmax above 25.6°C, followed by frequently inundated low and mid-fresh-oligohaline marshes with MATmax ≤25.6°C, and mesohaline sites with MATmax above 19°C. Methane fluxes at sites with salinities >18 psu were consistently low regardless of MATmax or elevation class (Figure 4). The representation of elevation classes was similar among fresh-oligohaline systems with MATmax ≤25.6°C, mesohaline sites with MATmax ≤19°C, and polyhaline and mixoeuhaline marshes (Figure S8). However, elevation could not be assessed as a predictor of annual $CH_4$ fluxes at warmer fresh-oligohaline (>25.6°C) and mesohaline (>19°C) sites due to the lack of variation in elevation classes within these categories.

While the mean difference between predicted and observed values was roughly equal to the average of annual $CH_4$ fluxes across the dataset, CTree binary partitioning enabled a breakdown of annual $CH_4$ fluxes across marsh categories based on salinity and daily maximum annual temperature, with additional consideration of elevation class specifically within the fresh-oligohaline category (Table 3).

### 3.3.2 | Predictors of $CH_4$ fluxes from disaggregated chamber data

We used chamber-based disaggregated data to understand $CH_4$ flux variability across sites and to establish quantitative relationships between $CH_4$ fluxes and predictor variables, particularly porewater biogeochemistry. Results from GAM models showed that porewater $CH_4$, porewater sulfate concentrations, and porewater salinity explained the highest percentage of the variance (27%–16%), followed by surface water salinity and air temperature (13%–8%) (Table 4). Similar results were obtained if $CH_4$ flux data were filtered to consider emissions only (i.e., $CH_4$ fluxes >0) (Table S7). Surface and porewater nitrate concentrations and porewater temperature also explained some percentage of the deviance in $CH_4$ fluxes (26%, 10%, and 18%, respectively); however, these results were based on a limited number of studies ($n < 5$) (Table S7). Adding study ID as a random

TABLE 3 Summary of annual $CH_4$ fluxes (g $CH_4$ $m^{-2}$ $year^{-1}$) grouped by salinity class, MATmax, and elevation class from the Conditional Inference Tree in Figure 4.

| Salinity class | MAT max | Elevation class | N | Distribution | Mean | SD | SE | Median | Geom. mean | geoSD |
|---|---|---|---|---|---|---|---|---|---|---|
| Fresh-oligohaline | >25.6 | | 7 | Normal | 171.5 | 79.4 | 30 | 204 | 153 | 1.7 |
| Fresh-oligohaline | ≤25.6 | Low, mid | 20 | Square root-normal | 54.9 | 56 | 12.5 | 41.5 | 15 | 10.5 |
| Fresh-oligohaline | ≤25.6 | High | 10 | Log-normal | 5.3 | 6.3 | 2 | 3.2 | 3.8[a] | 2.7 |
| Mesohaline | >19 | | 8 | Log-normal | 21.5 | 19.5 | 6.9 | 19.2 | 15.8 | 2.3 |
| Mesohaline | ≤19 | | 39 | Log-normal | 6.9 | 10.3 | 1.7 | 3.1 | 3.4[a] | 3.6 |
| Poly-mixoeuhaline | | | 24 | Log-normal | 1.8 | 2.3 | 0.5 | 0.7 | 1.2[a] | 2.9 |

Note: *N* is number of sites, SD and SE are standard deviation and error, respectively, geom.mean refers to geometric mean, and geoSD is the standard deviation of the latter.

[a]Negative flux values ($n=1$ high fresh-oligohaline ≤25.6; $n=1$ mesohaline ≤19°C) and fluxes equal to zero ($n=1$; mesohaline ≤19°C; $n=3$ poly-mixoeuhaline) were removed to compute the geometric mean.

TABLE 4 General additive model (GAM) results for chamber-disaggregated $CH_4$ fluxes against time-specific predictor variables.

| Variable | $R^2$ | Deviance explained (%) | d.f. | AIC | # studies |
|---|---|---|---|---|---|
| Porewater $CH_4$ | 0.27 [0.33] | 27 [34] | 879 | 8420 [8336] | 11 |
| Porewater $SO_4^{2-}$ | 0.21 [0.27] | 22 [29] | 310 | 4200 [4177] | 6 |
| Porewater salinity | 0.16 [0.20] | 16 [22] | 1162 | 16,734 [16,680] | 15 |
| Surface water salinity | 0.12 [0.46] | 13 [46] | 760 | 9463 [9088] | 6 |
| Air temperature | 0.08 [0.26] | 8 [26] | 6729 | 88,747 [87,337] | 28 |
| cosHour | 0.05 [0.32] | 5.1 [32] | 6229 | 85,370 [83305] | 18 |
| Porewater $SO_4^{2-}$ and porewater $CH_4$ | 0.67 [0.71] | 69 [73] | 239 | 2097 [2065] | 5 |
| Surface water salinity and air temperature | 0.60 [0.66] | 61 [67] | 654 | 7632 [7514] | 5 |
| Porewater salinity and porewater $CH_4$ | 0.32 [0.36] | 34 [39] | 347 | 3594 [3576] | 7 |

*Notes*: In brackets are GAM results with Study ID as a random effect. Results shown include relationships that explain >5% of the deviance in $CH_4$ fluxes, focusing on variables available in at least five studies. Table S7 contains GAM results for $CH_4$ emissions (i.e., >0) against all time-specific predictor variables with a significant relationship ($p<.05$). d.f. stands for degrees of freedom, AIC is the Akaike information criterion, and # studies indicate the number of studies that recorded each predictor variable (the total number of studies is 35).

effect increased the model performance between 6 and 32%, with the lowest increase observed for porewater salinity and the highest increase observed for surface water salinity. This highlights the intrinsic site-specific variability of $CH_4$ fluxes when predicted using surface water salinity. It also emphasizes the disconnect between surface and porewater salinity. Multivariate GAM models combining porewater $CH_4$ and sulfate concentrations, or surface salinity and air temperature, achieved the best performance with the highest deviance explained, 73% and 67%, respectively. However, these models were representative of only five studies (Table 4).

To estimate effect sizes, we examined the individual relationships between $CH_4$ fluxes and porewater concentrations of $CH_4$, sulfate, and salinity. All these variables, except for porewater $CH_4$, had significant effects on the magnitude of $CH_4$ fluxes, as shown by nonlinear quantile regression fits (Figure 5; Table S8). We observed a significant exponential decrease in $CH_4$ fluxes as surface and porewater salinity or sulfate concentrations increased. Moreover, as salinity and sulfate concentrations increased, the range of $CH_4$ fluxes decreased, suggesting that the effects of salinity and sulfate on $CH_4$ emissions were not consistent across all study sites. At the median quantile, $CH_4$ fluxes were significantly reduced when porewater sulfate and porewater salinity exceeded $2.8\pm0.5$ mM and $9.6\pm1.1$ psu, respectively. A 90% response, indicated by a significant reduction of the 0.9 quantile of the $CH_4$ fluxes, was achieved when sulfate concentrations reached $4.7\pm0.6$ mM, and porewater and surface water salinity reached $21\pm2$ and $15\pm3$ psu, respectively (Figure 5). These values represent the mean estimated cutoff points below which either the 50% or 90% of the highest $CH_4$ fluxes occur.

Analysis of the quantile regression model residuals revealed that $CH_4$ fluxes were not dependent on only one predictor variable. Several environmental covariates could explain variability in model residuals of the porewater or surface water salinity-$CH_4$ relationship. Primarily, the residual variance in $CH_4$ fluxes modeled from surface water salinity was notably influenced by porewater sulfate and $CH_4$ concentrations. Likewise, sulfate concentrations and porewater temperature influenced the remaining variance in fluxes modeled

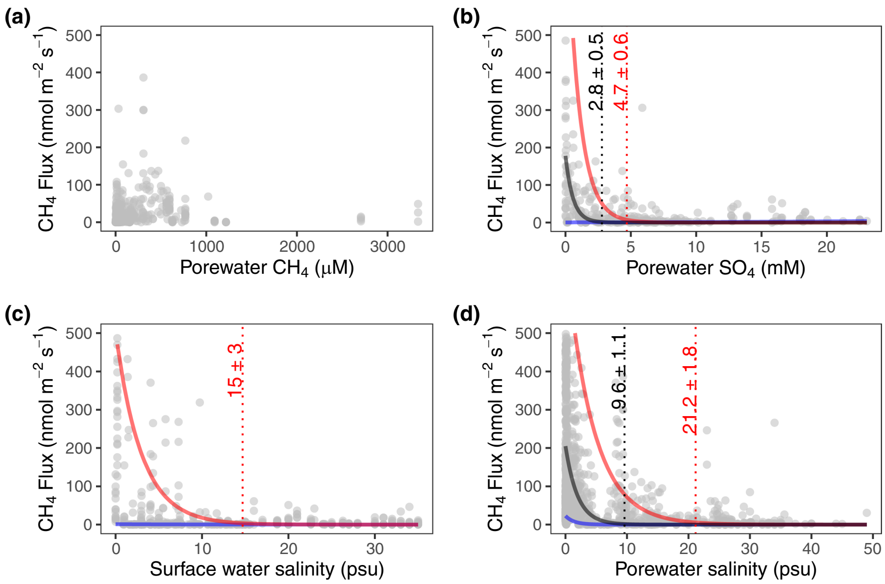


**FIGURE 5** Quantiles of $CH_4$ fluxes as a function of best-ranked predictors in general additive models with the solid blue, black, and red lines representing the fitted regression for the 0.1, 0.5, and 0.9 quantiles of $CH_4$ fluxes, respectively. Only lines for significant fits are shown. Statistics for the regression lines are summarized in Table S8. Vertical dashed lines represent thresholds of predictor variables below which the highest 50% and 90% of $CH_4$ fluxes occur. Data in the figure represent chamber-based $CH_4$ fluxes disaggregated by sampling event with matching porewater data. Points with emissions above 500 nmol m$^{-2}$ s$^{-1}$ are not displayed.

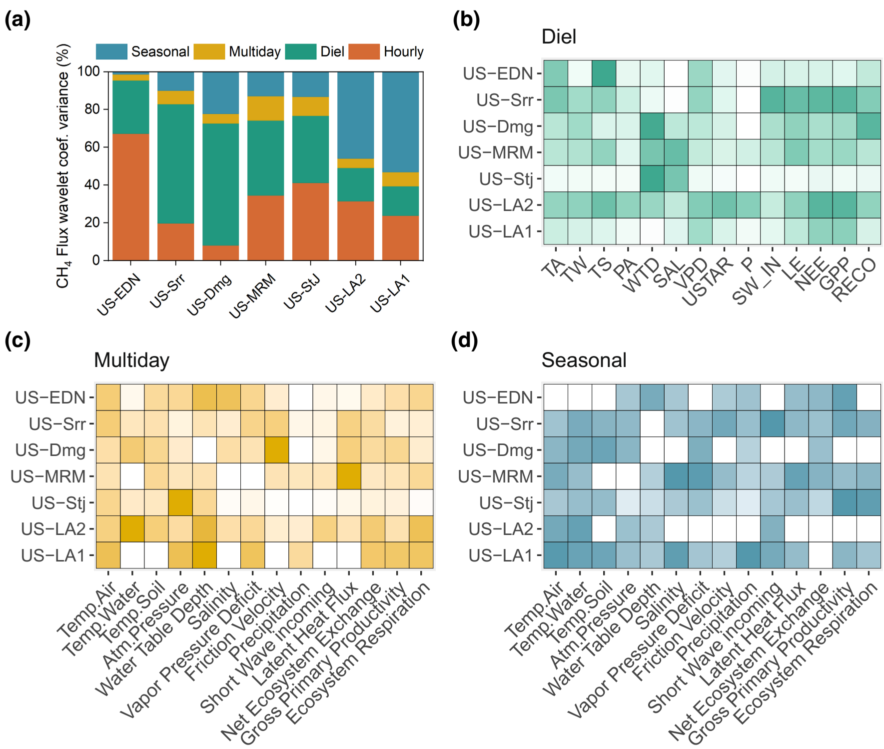


**FIGURE 6** Variance of $CH_4$ flux and dominant predictor variables across timescales. Variance of $CH_4$ flux wavelet coefficients at each timescale of interest as a percentage of the total variance for all eddy covariance tower sites with at least a full year of gap-filled data (a). Heatmap of normalized (0 to 1 scale), maximum relative mutual information ($I^R$) between methane flux and biophysical variables within sites for the (b) diel, (c) multiday, and (d) seasonal scale. All analyses were conducted on wavelet-transformed data. Light colors represent the lowest normalized $I^R$, dark colors the highest normalized $I^R$ and non-significant $I^R$ values are shaded white. See Table S1 for tower site information. Predictor codes in (b) are spelled out in panels (c) and (d).

from porewater salinity (Figures S9 and S10). In contrast, no predictor variable was found to explain the variability in model residuals of the sulfate-$CH_4$ flux relationship.

## 3.4 | Predictors of $CH_4$ flux across timescales

Mutual Information analysis using wavelet decomposed EC datasets revealed that $CH_4$ responses to environmental covariates exhibited nonlinearity and were characterized by asynchronous interactions, particularly at the multiday and seasonal scales (compare maximum $I^R$ heatmaps in Figure 6 with those of synchronous $I^R$ in Figure S11).

The diel timescale generally dominated $CH_4$ flux variability across tidal marsh EC sites, except for microtidal sites in Louisiana (US-LA1 and US-LA2), where the seasonal scale prevailed (Figure 6a). For some sites, the proportion of variance in $CH_4$ flux at the hourly scale appeared large (e.g., US-EDN). This was generally due to the higher signal-to-noise ratio at sites with low $CH_4$ fluxes or their low variation at other scales. The variance in $CH_4$ fluxes at the multiday scale was the lowest across all tidal marsh EC sites.

To assess the relative importance of $CH_4$ flux predictors at each timescale, we first normalized relative mutual information ($I^R$) values (Figure S12) within each site and then averaged normalized $I^R$ across sites. We did that within each timescale of interest (Figure 6b–d). At the diel scale, the main predictors of $CH_4$ flux were GPP, net ecosystem exchange, and soil temperature. Latent heat and water table depth ranked 4th and 5th in importance. On a multiday scale, the hierarchy of predictors was led by air temperature, water table depth, and atmospheric pressure. At the seasonal scale, water and air temperature were among the top predictors, followed by GPP and incoming shortwave radiation. Vapor pressure deficit and salinity ranked 5th and 6th, respectively, while water table depth was last in importance.

Heatmaps in Figure 6b–d provide a more detailed depiction of the primary predictors determined by maximum $I^R$ between $CH_4$ flux and biophysical variables. These heatmaps reveal site-specific patterns not evident when averaging normalized $I^R$ values across sites. Notably, water table depth and GPP emerged as dominant predictors at sites with large $CH_4$ flux variance at the diel scale. Diurnal patterns, characterized by peak $CH_4$ fluxes during midday hours and lower fluxes at night, as well as pulses of $CH_4$ flux occurring within 0 and 90 min after low tide, were commonly observed at these sites (Figures 7a–c and S13). On a multiday scale, increased $CH_4$ fluxes aligned with either spring tide cycles (US-EDN) or atmospheric pressure lows (US-LA1, US-LA2, US-StJ). At the seasonal scale, the dominance of water and air temperature, followed by GPP was apparent in most sites (Figure 6c). In some cases, lows in dissolved oxygen (at US-StJ) or high precipitation, bringing pulses of fresh water (US-LA1), manifested as key controls of $CH_4$ flux (Figure 7g,i).

While the influence of temperature (air, soil, or water) and effects of plant activity (through GPP, net ecosystem exchange or latent heat) on $CH_4$ fluxes were apparent across timescales and sites, the presence of a diel cycle marked by plant activity was site-specific. Heatmaps in Figure 6 support the point that there may not be a universal explanation for flux variability; rather, $CH_4$ fluxes appear to be conditional on time and location. Salinity was not a top predictor in continuous EC datasets when averaging normalized $I^R$ values across sites. However, it emerged as an important predictor at the seasonal timescale at sites that experienced a freshening during the growing season months (US-LA1, US-MRM, and US-EDN) (Figure S14), or at the diel scale where it correlated with water table depth (US-StJ or US-MRM).

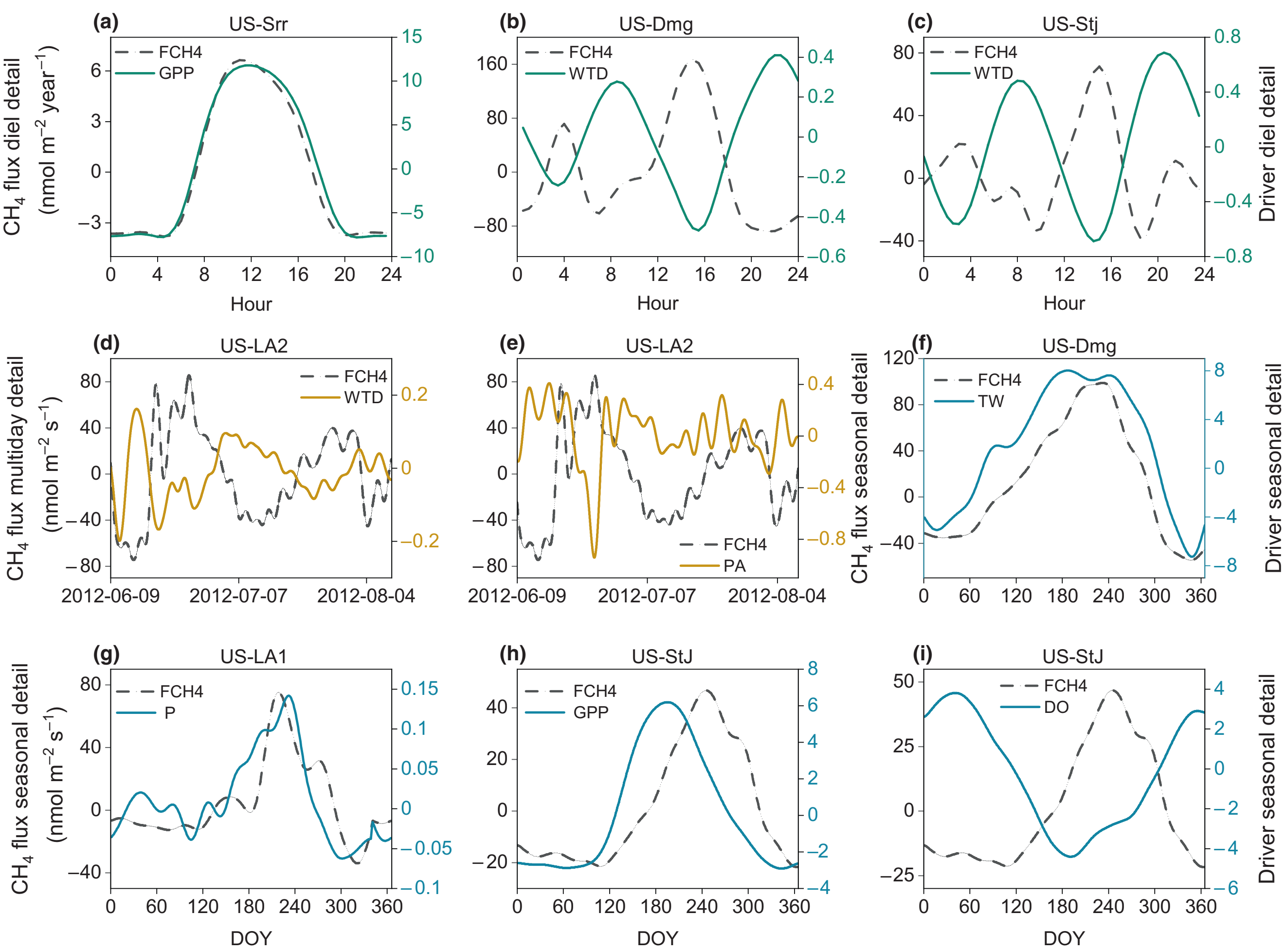


**FIGURE 7** Examples of diel and seasonal variation in the wavelet detail reconstruction for $CH_4$ flux and predictor variables. Note that the mean is removed in wavelet detail reconstructions; therefore, the y-axes are relative rather than absolute. Panels (a) through (c) illustrate diel wavelet details, panels (d) and (e) show examples of multiday wavelet details, and panels (f) through (i) show seasonal wavelet details. Predictor variable abbreviations are those introduced in Figure 6. DO stands for dissolved oxygen. Wavelet details for $CH_4$ flux, water table depth, and salinity at the diel and seasonal scales across all eddy covariance sites are in Figures S13 and S14, respectively.

## 4 | DISCUSSION

Our primary goal was to improve predictions of $CH_4$ emissions from tidal marshes in CONUS. This discussion focuses on four research questions that align with this goal. Firstly, we identify the primary predictors of $CH_4$ flux in tidal marshes across sites using broadly available data. Secondly, using EC sites with continuous $CH_4$ flux data, we assess the effects of predictors across varying timescales. Third, we discuss the application of scaling factors to annualize short-term static chamber measurements and their limitations, considering daily and seasonal flux variations. Lastly, we highlight how the identified relationships and gained information can be applied to improve monitoring and predictions of $CH_4$ emissions in tidal marshes, supporting blue carbon assessments and advancing our ability to constrain estimates of GHG emissions across diverse tidal wetlands.

### 4.1 | Dominant predictors of $CH_4$ flux in tidal marshes across CONUS

In our analysis of tidal marsh $CH_4$ fluxes across CONUS, we observed a wide range of flux magnitudes, varying from −150 to 4120 nmol m$^{-2}$ s$^{-1}$, with an average of 82 nmol m$^{-2}$ s$^{-1}$ and a median significantly lower at 5.8 nmol m$^{-2}$ s$^{-1}$. When compared to available estimates from a recent synthesis, the median instantaneous $CH_4$ flux per unit area aligns with values reported for North American saltmarshes, yet it is approximately half of that observed for mangroves, and about 10 times higher than figures reported for seagrasses (Rosentreter et al., 2023). Annual $CH_4$ fluxes showed a positive skew with a mean of 26 ± 53 g $CH_4$ m$^{-2}$ year$^{-1}$ and median and geometric means significantly lower, a reflection of the predominant data from mesohaline tidal marshes as well as the notoriously variable behavior of $CH_4$, with hotspots of activity. This raises a question about the reliability of arithmetic, median, or geometric mean values as estimates for representing the regional scale magnitude of annual $CH_4$ emissions in tidal marshes or their emission factors globally. The adequacy of these metrics will largely depend on the actual distribution and proportion of various marsh salinity classes across different climatic zones (e.g., Table 3). However, at finer spatial and temporal scales, factors such as hydrology, plant activity, and porewater biogeochemistry may become more influential than salinity in determining tidal marsh $CH_4$ fluxes.

#### 4.1.1 | Influence of salinity, temperature, relative elevation, and alternate electron acceptors on $CH_4$ fluxes

Across CONUS, we observed significant differences in median annual $CH_4$ fluxes among salinity classes, with a ~ threefold decrease in median $CH_4$ fluxes for each increase in salinity class from fresh to mixoeuhaline (Figure 3b). Median $CH_4$ fluxes in tidal freshwater marshes were 2, 8, 29, and 69 times higher than those of oligohaline, mesohaline, polyhaline, and mixoeuhaline marshes, respectively. Previous studies by Bartlett et al. (1987) and Poffenbarger et al. (2011) demonstrated a significant relationship between $CH_4$ fluxes and salinity. Sites with salinities above 18 psu had significantly lower $CH_4$ fluxes than less saline marshes, but this relationship was found to be less predictive at sites with salinities fresher than 18 psu (Poffenbarger et al., 2011; Windham-Myers et al., 2018). This agrees with our results when data were summarized at the annual level. When examining the data at the disaggregated level, $CH_4$ fluxes from freshwater and oligohaline marshes (0–5 psu) were the only groups showing statistical overlap (Figure 3c). This suggests that the attenuation of $CH_4$ fluxes by salinity primarily occurs beyond the oligohaline threshold (>5 psu) and that variables other than salinity may dominate $CH_4$ flux variance in fresh-oligohaline conditions.

Consistent with Poffenbarger et al. (2011), who found substantial dispersion in annual $CH_4$ fluxes at low salinities below 5 psu, we observed a great deal of variation in $CH_4$ fluxes with the magnitude of the variance decreasing as salinity increased (Figure 3b,c). At fresh to mesohaline sites, variability in annual $CH_4$ fluxes was partially attributed to temperature. Additionally, elevation class, a qualitative measure of inundation frequency, also contributed to the variability in annual $CH_4$ fluxes across fresh-oligohaline sites. The highest fluxes were observed at fresh and oligohaline sites experiencing a daily maximum annual temperature normal (MATmax) above 25.6°C (~204 g $CH_4$ m$^{-2}$ year$^{-1}$). These were followed by frequently inundated low and mid-fresh-oligohaline marshes with MATmax ≤25.6°C (~42 g $CH_4$ m$^{-2}$ year$^{-1}$), and mesohaline sites with MATmax above 19°C (~19 g $CH_4$ m$^{-2}$ year$^{-1}$) (Table 3). The fact that elevation class emerged as an important explanatory variable for $CH_4$ fluxes at low salinity levels may reflect the decrease in soil oxygen availability as flooding increases from high to low elevations (Kirwan et al., 2013), enhancing methanogenesis and suppressing methanotrophy. This pattern, however, did not emerge in saline systems, possibly due to the overriding influence of sulfate availability compared to fresh sites (DeLaune et al., 1983; Martens & Berner, 1974). In saline environments, $CH_4$ fluxes could remain low regardless of inundation, as sulfate reduction precedes methanogenesis. However sample size limitations and high variability within groups could have also played a role.

Synthesizing chamber-disaggregated flux and ancillary variables by sampling event allowed us to evaluate further the effects of salinity, temperature, and porewater biogeochemistry on the magnitude and variability of $CH_4$ fluxes in tidal wetlands. As per the well-established $CH_4$ response to salinity observed in other studies (Bartlett et al., 1987; DeLaune et al., 1983; Poffenbarger et al., 2011; Sanders-Demott et al., 2022; Schultz et al., 2023; Windham-Myers et al., 2018), chamber flux data disaggregated by sampling event also showed a significant exponential decrease with increasing salinity, for both surface water and porewater (Figure 5c,d). Across the range of sites, fitted median $CH_4$ fluxes fell below 1.6 ± 1.3 nmol m$^{-2}$ s$^{-1}$ at porewater salinities above 9.6 ± 1.1 psu. However, some instances of high $CH_4$ emissions

(50–170 nmol $m^{-2}$ $s^{-1}$) were still evident above this threshold. A more conservative threshold was identified at porewater salinities of 21 ± 2 psu, incorporating the 90th percentile of the $CH_4$ fluxes. The latter threshold was 15 ± 3 psu if surface water salinity was considered instead. Surface water and porewater salinity are not always well correlated at a site, as surface water salinity is often more variable than porewater salinity (Wilson et al., 2015). Indeed, the salinity measured on the surface may not accurately reflect the salinity conditions experienced by methanogens or, more precisely, their competition with sulfate-reducing bacteria. Surface inputs of salts are modified by plant transpiration, while sulfate inputs are modified by the balance between consumption by sulfate-reducing bacteria and production by sulfide oxidation. Such process may explain the reduced predictability of $CH_4$ emissions when using surface water salinity as a standalone predictor; thus, porewater salinity is preferred. Methane emissions significantly decreased with increasing porewater salinity across all conditional quantile levels, whereas surface salinity only explained changes in $CH_4$ emissions at the 90th percentile of the flux distribution (Table S8; Figure 5).

Causes of $CH_4$ flux variation at low salinities have previously been explained by microsite spatial and temporal variability in the presence of alternate electron acceptors and the sensitivity of methanogens to variations in their availability (Brooker et al., 2014; Galand et al., 2003). Because of the high abundance of sulfate in seawater, salinity has been used as a proxy of sulfate availability in tidal and salt marsh studies. However, we observed considerable variability in sulfate concentrations at a given salinity level, particularly when surface salinity was used to infer porewater sulfate concentrations (Figure S15a,b). Sulfate concentrations can change independently of salinity due to local sulfate depletion, leading to high $CH_4$ emissions despite high salinity levels, as observed in Wilson et al. (2015), and at high (>10 psu) porewater salinities in this synthesis (Figure 5d).

The general inverse relationship between sulfate concentration and $CH_4$ emissions is well-supported and upheld by studies through time (Bartlett et al., 1987; DeLaune et al., 1983; Martens & Berner, 1974; Poffenbarger et al., 2011). However, it is not well defined if there is a specific sulfate concentration above which tidal marsh $CH_4$ emissions are negligible. Poffenbarger et al. (2011) found that porewater $CH_4$ concentrations were negligible at sulfate concentrations >4 mM in marsh soils. However, they did not relate porewater sulfate concentration to $CH_4$ emissions due to the lack of paired data to evaluate such a relationship. Our analysis suggests that median $CH_4$ emissions were low across sites at porewater sulfate concentrations >2.8 ± 0.5 mM. However, considering the large spread of the response of $CH_4$ emissions to sulfate at low (<5 mM) sulfate concentrations, a more stringent threshold of 4.7 ± 0.6 mM delineated $CH_4$ emissions in the lowest 90th percentile of the data (Figure 5b). $CH_4$ emissions displayed significant responses to sulfate concentrations at all quantile levels and exhibited a third of the residual variance observed in $CH_4$ flux responses to porewater salinity. Residual analysis revealed that the modeled salinity–$CH_4$ relationship tended to overestimate $CH_4$ emissions as porewater sulfate concentrations decreased, particularly within 0 to 5 mM, indicating a greater sensitivity to increasing sulfate availability than to increasing salinity. A similar trend was observed for residuals fitted to porewater $CH_4$ concentrations, particularly within the range 0–100 μM $CH_4$, highlighting the activity of sulfate reducers as a primary control on $CH_4$ production in surface soils (0–30 cm).

We did not find a consistent significant relationship between porewater $CH_4$ concentrations and $CH_4$ fluxes (Figure 5a; Table S8). The discrepancy between $CH_4$ production and emissions may be attributed to several factors. These include bacterial-mediated aerobic $CH_4$ oxidation near the sediment surface during low tide or facilitated by plant rhizosphere oxygenation (Megonigal & Schlesinger, 2002; Van der Nat & Middelburg, 1998). Additionally, non-diffusive emission pathways like ebullition and plant-mediated transport (Hill & Vargas, 2022) are not always accounted for in chamber studies, as chambers may not include tall vegetation or headspace concentrations may be filtered to remove pulsed or erratic emissions. Furthermore, tidal flooding could drive lateral transport of dissolved porewater $CH_4$ from the marsh, which would be missed by chamber and eddy flux methods (Kelley et al., 1995; Tong et al., 2010; Trifunovic et al., 2020).

Porewater nitrate concentrations are typically low in most coastal marshes (Valiela & Teal, 1974), but surface water concentrations can be notably high at some sites due to agricultural intensification and other anthropogenic sources (Galloway et al., 2003; Pardo et al., 2011) (Figure S15). Nitrate is a thermodynamically favorable electron acceptor used by anaerobic bacteria shown to enhance soil organic matter decomposition (Bulseco et al., 2019). Similarly to sulfate, methanogenesis can be inhibited in the presence of nitrate. In this synthesis, signals of this process might be observed from the decrease in EC and chamber-based $CH_4$ fluxes with increasing dissolved nitrate concentrations (Figure S15c,d). However, the extent of $CH_4$ emission reduction was less pronounced for nitrate than for porewater sulfate. This pattern emerged despite a small dataset ($n$ = 3 studies), suggesting that nitrate inhibition of methanogenesis by nitrate reducers (denitrifiers) is a very strong biogeochemical signal that should be explored further given the fact that the process may also produce nitrous oxide ($N_2O$), a potent GHG. Our dataset lacked contemporaneous measurements of $N_2O$ emissions at these sites.

## 4.2 | Tidal marsh $CH_4$ fluxes across timescales

Methane fluxes in tidal marshes, as measured by EC, exhibited strong variation at the diel scale (Figure 6a), although most of the CONUS sites experience a strongly seasonal temperate climate. Among the seven EC sites analyzed, US-Srr exhibited a unique diel pattern in $CH_4$ flux wavelets. Peak fluxes occurred from late morning to mid-afternoon and were correlated with GPP, net ecosystem exchange, or incoming shortwave radiation. This pattern was likely due to its high marsh elevation, not frequently inundated in the flux footprint. In contrast, most sites showed less symmetric diel patterns influenced by diurnal and tidal interactions, with additional peaks often lagging lows of sinusoidal tidal patterns (Figure 7a–c; Figure S13), representing the release of stored $CH_4$ during brief and localized periods at low tide.

Higher daytime $CH_4$ fluxes could stem from several factors, increased soil and air temperatures (Bansal et al., 2018), enhanced root exudation with GPP stimulating methanogens and microbial priming (Bridgham et al., 2013), or $CH_4$ transport mediated by plants. This plant-mediated transport could either be driven by a pressure gradient that intensifies during daylight and coincides with active photosynthesis (Bansal et al., 2020; Dacey & Klug, 1979; Vroom et al., 2022) or by stomatal control of diffusive transport (Garnet et al., 2005). The former might be particularly relevant in *Phragmites*-dominated marshes (van den Berg et al., 2020; Van der Nat & Middelburg, 1998). Evidence from local studies focusing on individual site locations suggested that both impoundment and *Phragmites* invasion, separately or combined, could markedly increase $CH_4$ fluxes (Martin & Moseman-Valtierra, 2015; Mueller et al., 2016; Sanders-Demott et al., 2022).

The dominance of the diel scale over the seasonal scale in $CH_4$ flux variance is not limited to EC sites included in this synthesis; it has also been documented in other tidal ecosystems, such as in a subtropical estuarine mangrove (Liu et al., 2022). Chamber studies that conducted measurements over 12–24 h periods or consisted of automated chambers also noted diel $CH_4$ fluctuations of varying frequency and nature. For instance, Kelley et al. (1995) noted that $CH_4$ fluxes were higher when tidal waters were closest to the soil surface. Diefenderfer et al. (2018) observed that $CH_4$ flux was greater at night, likely due to the effects of hydrostatic pressure on diffusion and ebullition processes influenced by water surface elevation dynamics. Capooci and Vargas (2022) found that confluences of peak daily temperatures and low to rising tides could cause $CH_4$ pulses throughout the day. Tong et al. (2013) reported that plant activity controlled $CH_4$ emissions during neap tide days when sites were exposed; when sites were flooded, other factors dominated. These findings suggest that while diel $CH_4$ flux variability is expected in tidal marshes, the presence and strength of a daily cycle are site-specific depending on species, temperature, and tidal forcings.

Microtidal sites in Louisiana do not experience large tidal amplitudes nor the sinusoidal pattern with tides; thus, peaks in wavelet analysis were not observed at diel scales related to semidiurnal tides or fortnightly neap-spring tidal cycles (Figure S13). Sites in Louisiana are wind- and river-influenced, and atmospheric pressure changes and freshwater pulses driven by synoptic and mesoscale weather played a more significant role in $CH_4$ flux variability. These results suggest that $CH_4$ fluxes and their drivers at microtidal sites may align more closely with those of non-tidal wetlands found elsewhere (Knox et al., 2021; Sturtevant et al., 2016). In contrast, where tides are significant, they may strongly modulate the timing and pathway of $CH_4$ emissions.

At the seasonal scale, water and air temperatures were the primary predictors of $CH_4$ flux, followed by GPP. Salinity ranked 6th in importance, demonstrating greater relevance at this scale compared with other timescales. This may reflect the limitations of using surface water salinity at EC sites to explain diel $CH_4$ flux responses. It may also suggest that seasonal, rather than shorter-term diel changes in surface water salinity are required to affect $CH_4$ emissions significantly. Seasonal salinity changes, driven by reduced freshwater flow and increased seawater intrusion, typically elevate salinity during the summer and growing season. However, higher temperatures and enhanced GPP during these periods could offset potential $CH_4$ flux inhibition due to increased sulfate availability. A distinct observation was that $CH_4$ fluxes were largely enhanced when reduced salinity aligned with peak growing season conditions (Figure 7; Figure S14).

### 4.3 | Daytime chamber $CH_4$ fluxes: Temporal upscaling and limitations

Only a few chamber studies have shown the significant variability of $CH_4$ fluxes at daily scales (Capooci & Vargas, 2022; Diefenderfer et al., 2018; Kelley et al., 1995; Tong et al., 2013), highlighting the limitations of temporally upscaling $CH_4$ fluxes from discrete static chamber measurements (Hill & Vargas, 2022; Vargas & Le, 2023). Static chambers, predominantly deployed at low tide, are limited in their sensitivity to sudden pulse events and may not effectively capture $CH_4$ responses to GPP dynamics. Assessments of GPP require consecutive measurements under both light and dark conditions that can be affected by chamber heating or an incomplete physiological adaptation (e.g., stomatal closure) to dark conditions. While static chamber measurements offer the advantage of capturing $CH_4$ flux variability across sites, they are not well suited to capture the temporal variability of $CH_4$ fluxes and their influencing factors.

However, most flux measurements in tidal marshes are derived from static chambers, often paired with sporadic recordings of temperature, water table depth, or porewater geochemistry. Lacking continuous predictor variables that would allow for confident temporal scaling of discrete $CH_4$ flux measurements, we estimated scaling factors based on sites with a full year of sampling coverage. Significant differences emerged between factors derived from EC (s.f. = 0.32) and chamber (s.f. = 0.39) methods when cumulative annual fluxes were compared against daily measurements averaged year-round. Daytime static chamber measurements hardly integrate diel variations in $CH_4$ fluxes, which likely introduces bias into annual estimates (Vargas & Le, 2023). Diel variations not only refer to fluctuations between day and night due to temperature and plant activity but can represent variations with tides, carbon substrates, and/or ebullition. At sites with overlapping chamber and EC measurements, chamber measurements were generally lower than EC, except at microtidal sites in Louisiana (Figure S16). This difference suggested that chamber measurements often miss episodic $CH_4$ flux events due to infrequent sampling and differing footprints, leading to site-level $CH_4$ flux discrepancies between methods. However, with chamber estimates of $CH_4$ fluxes ranging from less than half (Hill & Vargas, 2022) to about twice as high as EC estimates (Krauss et al., 2016), disparities appeared to be site-specific and difficult to reconcile at the regional level.

Building on the scaling factors discussed earlier, Bridgham et al. (2006) found a similar ratio between annual and mean daily $CH_4$ fluxes from chamber measurements in non-tidal freshwater (s.f. = 0.36) and estuarine (s.f. = 0.34) wetlands across North America, suggesting there is a ~360-day emission season. Seasonality in $CH_4$ fluxes is evident in many tidal wetland datasets (Figure S14a) (e.g., Derby et al., 2022; Neubauer, 2013; Vázquez-Lule & Vargas, 2021), with $CH_4$ fluxes typically being low during winter. However, a substantial fraction (~15%) of annual $CH_4$ fluxes may occur during cooler months, as observed in this study for sites with year-round data and in temperate freshwater wetlands in Delwiche et al. (2021). Specifically, in our dataset, $CH_4$ fluxes during January–March and October–December accounted for 9 ± 5% and 20 ± 6% of annual $CH_4$ fluxes, respectively, highlighting the significance of winter fluxes in the annual $CH_4$ budget.

Most static chamber studies in temperate marshes typically exclude winter sampling. Traditionally, a common approach was to annualize the average daily fluxes from the growing season, applying a 150-day emissions season and assuming negligible winter emissions (Bartlett & Harriss, 1993; Magenheimer et al., 1996). More recently, scaling factors, as described in Bridgham et al. (2006), have been used to calculate annual $CH_4$ fluxes from mean daily fluxes sampled during the growing season (Bridgham et al., 2006; Poffenbarger et al., 2011). However, this approach may lead to an apparent overestimation of annual $CH_4$ fluxes of up to ~50% due to the relative seasonal increase in $CH_4$ fluxes compared with baseline (Figure S17). According to our results, an emission season of 210 days (or s.f. = 0.21) may be more accurate to consider if fluxes are sampled during the peak emission period (June–August) (Figure 2). The variance of the June–August scaling factor across sites was lower than that observed for the ratio of annual flux: mean daily flux averaged year-round. Additionally, no significant differences were detected in the June–August scaling factors between chamber and EC sites. This might be due to the lower variability in within-site $CH_4$ fluxes during the peak emission season compared with that observed year-round. Consequently, the ratio of annual flux to June–August mean daily flux may be less affected by how well the length and amplitude of the seasonal cycle are captured by discrete chamber measurements.

## 4.4 | Advancing $CH_4$ flux assessments in tidal marshes

Results of the present study could improve predictions of $CH_4$ emissions in tidal marshes at the local and regional levels in various ways. Porewater sulfate and salinity concentration thresholds below which 90% of the highest $CH_4$ fluxes occur (4.7 ± 0.6 mM $SO_4^{2-}$ and 21 ± 2 psu, respectively) may help determine whether a site's $CH_4$ responses should be included in blue carbon assessments, wetland restoration monitoring, or GHG inventories. Above these thresholds, $CH_4$ emissions may be considered negligible. Despite porewater sulfate concentrations more accurately representing the competition between methanogens and sulfate-reducing bacteria, the practicality of porewater sulfate as a proxy for widespread application may be limited due to the challenges associated with its measurement. On the contrary, porewater salinity, which is relatively easy to measure and also represents conditions experienced by methanogens, could be more applicable in real-world scenarios for estimating the magnitude of $CH_4$ fluxes across a range of sites.

Estimated median annual $CH_4$ fluxes among salinity classes (Figure 3b), which showed a consistent ~threefold decrease for each increase in salinity class, could serve as CONUS-specific Tier 2 estimates, offering a more detailed approach to better constrain $CH_4$ emissions factors beyond the global Tier 1 factors of the IPCC Wetlands Supplement (IPCC, 2014). The current Tier 1 emission factor relies on an 18 psu salinity threshold, below which $CH_4$ emissions are set at 19 g $CH_4$ $m^{-2}year^{-1}$ (based on range 1.1–539 g $CH_4$ $m^{-2}year^{-1}$), and above it are set at zero. However, the primary limitation of the salinity–$CH_4$ flux relationship in predicting $CH_4$ fluxes lies in the substantial variability in flux magnitudes observed at low salinity conditions (< 18 psu). Our results suggest that the daily maximum annual temperature normal (MATmax), along with elevation class, could be used to improve the accuracy of this relationship. Table 3 proposes a new categorization of annual $CH_4$ fluxes that distinguishes between warmer and cooler fresh-oligohaline and mesohaline marshes. Additionally, it incorporates marsh elevation classes within fresh-oligohaline conditions to better constrain $CH_4$ fluxes at low salinity levels. This categorization, specific to US data, could further improve Tier 2 estimates. This approach would adjust median emission factors for fresh-oligohaline marshes with MATmax >25.6°C to be 8–10 times higher than the current Tier 1 factor, while those for frequently inundated, low- and mid-elevation fresh-oligohaline marshes with MATmax below 25.6°C would be increased by two times. Emission factors for warm mesohaline marshes (MATmax >19°C) would remain unchanged. Conversely, the revised median estimate for infrequently inundated colder fresh-oligohaline high marshes (MATmax ≤25.6°C), and mesohaline marshes (MATmax ≤19°C) would be one-sixth of the current Tier 1 factor. These emission factors could be viewed as Tier 2 estimates for implementing national inventories rather than precise predictions of tidal marsh $CH_4$ fluxes across temporal and spatial scales. Eddy covariance datasets identified GPP as a main predictor of $CH_4$ fluxes. If GPP data were available across more tidal marsh sites, it could improve annual $CH_4$ flux predictions and offer valuable insights for future studies. Likewise, the hydrologic setting, often reported qualitatively as either "high" or "low" marsh environments, could be made a stronger predictor of annual $CH_4$ fluxes across sites by including a quantitative metric of relative tidal elevation, such as elevation normalized to tidal amplitude in future research (e.g. $Z^*_{MHW}$, Holmquist & Windham-Myers, 2022).

Daytime chamber measurements during the growing season currently represent the majority of available $CH_4$ flux data from tidal wetlands and are likely to remain prevalent. Therefore, developing carbon exchange models that combine discrete chamber $CH_4$ fluxes with continuous predictor variables or robust scaling factors to annualize daytime chamber measurements would support the continuation of chamber monitoring approaches. This would enhance efforts to achieve Tier 2 national inventories and implement carbon finance protocols by reducing the data collection effort, which is generally less available than carbon sequestration data. Despite its limitations, we provide a scaling factor (s.f. = 0.21) that can be used to upscale growing season chamber-based $CH_4$ fluxes to first-order annual $CH_4$ flux estimates. However, we caution about the limitations of manual measurements in capturing the temporal variability of $CH_4$ fluxes. The presence and symmetry of a diel cycle appeared to be site-specific, suggesting that scaling factors should ideally be assessed carefully on a site-specific basis. We propose that when feasible, $CH_4$ flux measurements be collected over a 24-h cycle or continuously using automated chambers or EC towers to capture the diurnal variability of $CH_4$ flux, identify important site-specific drivers, and improve scaling factors.

## 5 | CONCLUSIONS

We compiled, standardized, and synthesized chamber-based $CH_4$ fluxes across tidal wetlands in CONUS and created an open-source database (Arias-Ortiz et al., 2024, https://doi.org/10.25573/serc.14227085). Chamber flux data disaggregated by sampling event combined with available EC datasets improved the representation of $CH_4$ fluxes and their variability across time and space in tidal marshes. Porewater sulfate and salinity, along with mean daily maximum annual temperatures and elevation, were important predictors of $CH_4$ emissions across sites. However, temperature, plant activity (through GPP), and tidal height significantly contributed to the variability of $CH_4$ fluxes within individual sites, with tidal height influencing the timing and pathways of $CH_4$ fluxes at the diel scale. Our analysis shows the large diel $CH_4$ flux variance observed in tidal wetlands, emphasizing the need for integrated measurement approaches to capture the complexity of tidal marsh $CH_4$ dynamics.

### AUTHOR CONTRIBUTIONS

**Ariane Arias-Ortiz:** Conceptualization; data curation; formal analysis; investigation; methodology; project administration; supervision; visualization; writing – original draft; writing – review and editing. **Jaxine Wolfe:** Conceptualization; data curation; methodology; software; visualization. **Scott D. Bridgham:** Conceptualization; investigation; methodology; writing – review and editing. **Sara Knox:** Conceptualization; formal analysis; methodology; software; writing – review and editing. **Gavin McNicol:** Conceptualization; methodology; writing – review and editing. **Brian A. Needelman:** Conceptualization; investigation; methodology; writing – review and editing. **Julie Shahan:** Formal analysis; investigation; methodology. **Ellen J. Stuart-Haëntjens:** Investigation; writing – review and editing. **Lisamarie Windham-Myers:** Conceptualization; funding acquisition; methodology; writing – review and editing. **Patty Y. Oikawa:** Conceptualization; investigation; methodology; project administration; writing – review and editing. **Dennis D. Baldocchi:** Investigation; methodology; software; supervision; writing – review and editing. **Joshua S. Caplan:** Data curation; investigation; writing – review and editing. **Margaret Capooci:** Data curation; investigation. **Kenneth M. Czapla:** Data curation; investigation; writing – review and editing. **R. Kyle Derby:** Data curation; investigation; writing – review and editing. **Heida L. Diefenderfer:** Data curation; investigation; writing – review and editing. **Inke Forbrich:** Data curation; investigation; writing – review and editing. **Gina Groseclose:** Data curation; investigation; writing – review and editing. **Jason K. Keller:** Data curation; investigation; writing – review and editing. **Cheryl Kelley:** Data curation; investigation; writing – review and editing. **Amr E. Keshta:** Data curation; investigation; writing – review and editing. **Helena S. Kleiner:** Data curation; investigation; writing – review and editing. **Ken W. Krauss:** Data curation; investigation; writing – review and editing. **Robert R. Lane:** Data curation; investigation; writing – review and editing. **Sarah Mack:** Investigation; writing – review and editing. **Serena Moseman-Valtierra:** Data curation; investigation; writing – review and editing. **Thomas J. Mozdzer:** Data curation; investigation; writing – review and editing. **Peter Mueller:** Data curation; investigation; writing – review and editing. **Scott C. Neubauer:** Data curation; investigation; writing – review and editing. **Genevieve Noyce:** Data curation; investigation; writing – review and editing. **Karina V. R. Schäfer:** Data curation; investigation; writing – review and editing. **Rebecca Sanders-DeMott:** Data curation; investigation; writing – review and editing. **Charles A. Schutte:** Data curation; investigation; writing – review and editing. **Rodrigo Vargas:** Data curation; investigation; writing – review and editing. **Nathaniel B. Weston:** Data curation; investigation; writing – review and editing. **Benjamin Wilson:** Data curation; investigation; writing – review and editing. **J. Patrick Megonigal:** Conceptualization; funding acquisition; investigation; methodology; project administration; writing – review and editing. **James R. Holmquist:** Conceptualization; funding acquisition; methodology; project administration; software; writing – review and editing.

### AFFILIATIONS

[1]Physics Department, Universitat Autònoma de Barcelona, Barcelona, Spain
[2]Ecosystem Science Division, Department of Environmental Science, Policy and Management, University of California, Berkeley, California, USA
[3]Smithsonian Environmental Research Center, Edgewater, Maryland, USA
[4]Institute of Ecology and Evolution, University of Oregon, Eugene, Oregon, USA
[5]Department of Geography, The University of British Columbia, Vancouver, British Columbia, Canada
[6]Department of Geography, McGill University, Montreal, Quebec, Canada
[7]Department of Earth and Environmental Sciences, University of Illinois Chicago, Chicago, Illinois, USA
[8]Department of Environmental Science and Technology, University of Maryland, College Park, Maryland, USA
[9]Earth System Science, Stanford University, Stanford, California, USA
[10]U.S. Geological Survey, Water Resources Mission Area, Menlo Park, California, USA
[11]Department of Earth and Environmental Sciences, California State University, East Bay, Hayward, California, USA
[12]Department of Architecture & Environmental Design, Temple University, Ambler, Pennsylvania, USA

[13]Department of Plant & Soil Sciences, University of Delaware, Newark, Delaware, USA
[14]Department of Environmental Sciences, University of California Riverside, Riverside, California, USA
[15]Maryland Department of Natural Resources, Chesapeake Bay National Estuarine Research Reserve, Annapolis, Maryland, USA
[16]Coastal Sciences Division, Pacific Northwest National Laboratory, Sequim, Washington, USA
[17]Ecosystems Center, Marine Biological Laboratory, Woods Hole, Massachusetts, USA
[18]Department of Environmental Sciences, University of Toledo, Toledo, Ohio, USA
[19]Department of Oceanography and Coastal Sciences, Louisiana State University, Baton Rouge, Louisiana, USA
[20]Schmid College of Science and Technology, Chapman University, Orange, California, USA
[21]Kravis Department of Integrated Sciences, Claremont McKenna College, Claremont, California, USA
[22]Department of Geological Sciences, University of Missouri, Columbia, Missouri, USA
[23]Botany Department, Faculty of Science, Tanta University, Tanta, Egypt
[24]Department of Environmental Science and Technology, University of Maryland, College Park, Maryland, USA
[25]U.S. Geological Survey, Wetland and Aquatic Research Center, Lafayette, Louisiana, USA
[26]Comite Resources, Baton Rouge, Louisiana, USA
[27]Tierra Resources LLC, Lafitte, Louisiana, USA
[28]Department of Biological Sciences, University of Rhode Island, Kingston, Rhode Island, USA
[29]Bryn Mawr College, Department of Biology, Bryn Mawr, Pennsylvania, USA
[30]Institute of Landscape Ecology, University of Münster, Münster, Germany
[31]Department of Biology, Virginia Commonwealth University, Richmond, Virginia, USA
[32]Earth and Environmental Science Dept, Rutgers University Newark, Newark, New Jersey, USA
[33]U.S. Geological Survey, Woods Hole Coastal and Marine Science Center, Woods Hole, Massachusetts, USA
[34]Department of Environmental Science, Rowan University, Glassboro, New Jersey, USA
[35]Department of Geography and the Environment, Villanova University, Villanova, Pennsylvania, USA
[36]Department of Biological Sciences, Florida International University, Miami, Florida, USA

## ACKNOWLEDGMENTS

This effort would not have been possible without the contributions of numerous collaborators, students, and technicians who created the original data sources at individual sites. Table *MWG_associated_publications* in the online database contains citations for all these individual works (https://doi.org/10.25573/serc.14227085). We thank the Coastal Carbon Network (CCN), all CCN Methane Working Group members, and original funding from NSF Research Coordination Network: DEB-1655622. We also acknowledge support from the Delta Stewardship Council, California (#21034 and #49861). AA-O was supported by the NOAA C&GC Postdoctoral Fellowship Program (#NA18NWS4620043B) and by a "Ramon y Cajal" Fellowship RYC2021-034455-I. GM was supported by the National Aeronautics and Space Administration (NASA), Carbon Monitoring System (#NNH20ZDA001N). LWM was supported by the USGS Water Resources Mission Area, and JRH was supported by NASA, Carbon Monitoring System (80NSSC20K0084), the Department of Energy project COMPASS-FME (DE-AC05-76RL01830), and the Smithsonian Institution. Table MWG_associated_funding in the online database lists support for individual projects that funded the data analyzed in this manuscript. Any use of trade, firm, or product names is for descriptive purposes only and does not imply endorsement by the US Government.

## CONFLICT OF INTEREST STATEMENT

The authors claim no conflicts of interest.

## DATA AVAILABILITY STATEMENT

Chamber flux data supporting the findings of this study are openly available in figshare at https://doi.org/10.25573/serc.14227085. Eddy covariance data is available at https://doi.org/10.6084/m9.figshare.26411305, from the FLUXNET-CH4 Community Product https://fluxnet.org/data/fluxnet-ch4-community-product/ or at AmeriFlux at https://ameriflux.lbl.gov/. DOIs for individual eddy covariance site data are provided in Table S1.

## ORCID

*Ariane Arias-Ortiz* https://orcid.org/0000-0001-9408-0061
*Patty Y. Oikawa* https://orcid.org/0000-0001-7852-4435
*Dennis D. Baldocchi* https://orcid.org/0000-0003-3496-4919
*Joshua S. Caplan* https://orcid.org/0000-0003-4624-2956
*Heida L. Diefenderfer* https://orcid.org/0000-0001-6153-4565
*Inke Forbrich* https://orcid.org/0000-0002-0632-7317
*Thomas J. Mozdzer* https://orcid.org/0000-0002-1053-0967
*Scott C. Neubauer* https://orcid.org/0000-0001-8948-2832
*Genevieve Noyce* https://orcid.org/0000-0003-0423-6478
*Charles A. Schutte* https://orcid.org/0000-0002-3907-7828
*Rodrigo Vargas* https://orcid.org/0000-0001-6829-5333
*Nathaniel B. Weston* https://orcid.org/0000-0002-6837-360X
*J. Patrick Megonigal* https://orcid.org/0000-0002-2018-7883
*James R. Holmquist* https://orcid.org/0000-0003-2546-6766

## REFERENCES

Abernethy, S., & Jackson, R. B. (2022). Global temperature goals should determine the time horizons for greenhouse gas emission metrics. *Environmental Research Letters*, *17*(2), 24019. https://doi.org/10.1088/1748-9326/ac4940

Al-Haj, A. N., & Fulweiler, R. W. (2020). A synthesis of methane emissions from shallow vegetated coastal ecosystems. *Global Change Biology*, *26*(5), 2988–3005. https://doi.org/10.1111/gcb.15046

Altor, A. E., & Mitsch, W. J. (2006). Methane flux from created riparian marshes: Relationship to intermittent versus continuous inundation and emergent macrophytes. *Ecological Engineering*, *28*(3 SPEC. ISS), 224–234. https://doi.org/10.1016/j.ecoleng.2006.06.006

Arias-Ortiz, A., Bridgham, S. D., Holmquist, J., Knox, S., McNicol, G., Needleman, B., Oikawa, P. Y., Stuart-Haëntjens, E. J., Windham-Myers, L., Wolfe, J., Anderson, I. C., Bailey, S., Baldwin, A., Bauer, C. E., Borde, A., Brady, L. J., Brewer, P., Brooks, W., Brophy, L., … Yarwood, S. (2024). Dataset: Chamber-based methane flux measurements and other greenhouse gas data for tidal wetlands across the contiguous United States - an open-source database. *Smithsonian Environmental Research Center*. https://doi.org/10.25573/serc.14227085

Bansal, S., Johnson, O. F., & Meier, J. (2020). Vegetation affects timing and location of wetland methane emissions. *Journal of Geophysical*

*Research – Biogeosciences*, *125*, e2020JG005777. https://doi.org/10.1029/2020JG005777
Bansal, S., Tangen, B., & Finocchiaro, R. (2018). Diurnal patterns of methane flux from a seasonal wetland: Mechanisms and methodology. *Wetlands*, *38*, 933–943. https://doi.org/10.1007/s13157-018-1042-5
Bartlett, K. B. (1985). Methane flux from coastal salt marshes. *Journal of Geophysical Research*, *90*(D3), 5710–5720.
Bartlett, K. B., Bartlett, D. S., Harriss, R. C., Sebacher, D. I., Biogeochemistry, S., & Sebacher, D. I. (1987). Methane emissions along a salt Marsh salinity gradient. *Biogeochemistry*, *4*(3), 183–202.
Bartlett, K. B., & Harriss, R. C. (1993). Review and assessment of methane emissions from wetlands. *Chemosphere*, *26*(1), 261–320. https://doi.org/10.1016/0045-6535(93)90427-7
Bendix, M., Tornbjerg, T., & Brix, H. (1994). Internal gas transport in Typha latifolia L. and Typha angustifolia L. 1. Humidity-induced pressurization and convective throughflow. *Aquatic Botany*, *49*(2–3), 75–89. https://doi.org/10.1016/0304-3770(94)90030-2
Bianchi, T. S. (2006). Chapter 13 carbon cycle. In T. S. Bianchi (Ed.), *Biogeochemistry of estuaries* (pp. 395–435). Oxford University Press.
Borde, A. B., Diefenderfer, H. L., Cullinan, V. I., Zimmerman, S. A., & Thom, R. M. (2020). Ecohydrology of wetland plant communities along an estuarine to tidal river gradient. *Ecosphere*, *11*(9), e03185. https://doi.org/10.1002/ecs2.3185
Breiman, L. (2001). Random forests. *Machine Learning*, *45*, 5–32. https://doi.org/10.1109/ICCECE51280.2021.9342376
Bridgham, S. D., Cadillo-Quiroz, H., Keller, J. K., & Zhuang, Q. (2013). Methane emissions from wetlands: Biogeochemical, microbial, and modeling perspectives from local to global scales. *Global Change Biology*, *19*(5), 1325–1346. https://doi.org/10.1111/gcb.12131
Bridgham, S. D., Megonigal, J. P., Keller, J. K., Bliss, N. B., & Trettin, C. (2006). The carbon balance of north American wetlands. *Wetlands*, *26*(4), 889–916. https://doi.org/10.1672/0277-5212(2006)26[889:TCBONA]2.0.CO;2
Brooker, M. R., Bohrer, G., & Mouser, P. J. (2014). Variations in potential CH4 flux and CO2 respiration from freshwater wetland sediments that differ by microsite location, depth and temperature. *Ecological Engineering*, *72*(December 2015), 84–94. https://doi.org/10.1016/j.ecoleng.2014.05.028
Bulseco, A. N., Giblin, A. E., Tucker, J., Murphy, A. E., Sanderman, J., Hiller-Bittrolff, K., & Bowen, J. L. (2019). Nitrate addition stimulates microbial decomposition of organic matter in salt marsh sediments. *Global Change Biology*, *25*(10), 3224–3241. https://doi.org/10.1111/gcb.14726
Cade, B. S., & Noon, B. R. (2003). A gentle introduction to quantile regression for ecologists. *Frontiers in Ecology and the Environment*, *1*(8), 412–420. https://doi.org/10.1890/1540-9295(2003)001[0412:AGITQR]2.0.CO;2
Call, M., Maher, D. T., Santos, I. R., Ruiz-Halpern, S., Mangion, P., Sanders, C. J., Erler, D. V., Oakes, J. M., Rosentreter, J., Murray, R., & Eyre, B. D. (2015). Spatial and temporal variability of carbon dioxide and methane fluxes over semi-diurnal and spring-neap-spring timescales in a mangrove creek. *Geochimica et Cosmochimica Acta*, *150*, 211–225. https://doi.org/10.1016/j.gca.2014.11.023
Campbell, B. J., & Kirchman, D. L. (2013). Bacterial diversity, community structure and potential growth rates along an estuarine salinity gradient. *ISME Journal*, *7*(1), 210–220. https://doi.org/10.1038/ismej.2012.93
Capooci, M., & Vargas, R. (2022). Trace gas fluxes from tidal salt marsh soils: Implications for carbon-sulfur biogeochemistry. *Biogeosciences*, *19*(19), 4655–4670. https://doi.org/10.5194/bg-19-4655-2022
Chmura, G. L., Anisfeld, S. C., Cahoon, D. R., & Lynch, J. C. (2003). Global carbon sequestration in tidal, saline wetland soils. *Global Biogeochemical Cycles*, *17*(4), 1111. https://doi.org/10.1029/2002gb001917
Chu, H., Christianson, D. S., Cheah, Y. W., Pastorello, G., O'Brien, F., Geden, J., Ngo, S. T., Hollowgrass, R., Leibowitz, K., Beekwilder, N. F., Sandesh, M., Dengel, S., Chan, S. W., Santos, A., Delwiche, K., Yi, K., Buechner, C., Baldocchi, D., Papale, D., … Torn, M. S. (2023). AmeriFlux BASE data pipeline to support network growth and data sharing. *Scientific Data*, *10*(1), 1–13. https://doi.org/10.1038/s41597-023-02531-2
Cloern, J. E., & Jassby, A. D. (2012). Drivers of change in estuarine-coastal ecosystems: Discoveries from four decades of study in San Francisco Bay. *Reviews of Geophysics*, *50*(4), 1–33. https://doi.org/10.1029/2012RG000397
Cornish, C. R., Percival, D. B., & Bretherton, C. S. (2003). The WMTSA Wavelet Toolkit for Data Analysis in the Geosciences. In *EOS Trans AGU* (Abstract NG11A-0173; Fall Meet. Suppl., Vol. 84, Issue 46).
Cowardin, L., Carter, V., Golet, F., & LaRoe, E. T. (1979). *Classification of wetland and deepwater habitats of the United States* (FWS/OBS-79/31). Fish and Wildlife Service, U.S. Department of the Interior, Washington, DC, pp. 103.
Dacey, J. W. H., & Klug, M. J. (1979). Methane efflux from lake sediments through water lilies. *Science*, *203*(4386), 1253–1255. https://doi.org/10.1126/science.203.4386.1253
DeLaune, R. D., Smith, C. J., & Patrick, W. H. (1983). Methane release from gulf coast wetlands. *Tellus B: Chemical and Physical Meteorology*, *35*(1), 8–15. https://doi.org/10.3402/tellusb.v35i1.14581
Delwiche, K. B., Knox, S. H., Malhotra, A., Fluet-Chouinard, E., McNicol, G., Feron, S., Ouyang, Z., Papale, D., Trotta, C., Canfora, E., Cheah, Y.-W., Christianson, D., Alberto, M. C. R., Alekseychik, P., Aurela, M., Baldocchi, D., Bansal, S., Billesbach, D. P., Bohrer, G., … Jackson, R. B. (2021). FLUXNET-CH$_4$: A global, multi-ecosystem dataset and analysis of methane seasonality from freshwater wetlands. *Earth System Science Data*, *13*(7), 3607–3689. https://doi.org/10.5194/essd-13-3607-2021
Derby, R. K., Needelman, B. A., Roden, A. A., & Megonigal, J. P. (2022). Vegetation and hydrology stratification as proxies to estimate methane emission from tidal marshes. *Biogeochemistry*, *157*(2), 227–243. https://doi.org/10.1007/s10533-021-00870-z
Diefenderfer, H. L., Cullinan, V. I., Borde, A. B., Gunn, C. M., & Thom, R. M. (2018). High-frequency greenhouse gas flux measurement system detects winter storm surge effects on salt marsh. *Global Change Biology*, *24*(12), 5961–5971. https://doi.org/10.1111/gcb.14430
Duarte, C. M., Losada, I. J., Hendriks, I. E., Mazarrasa, I., & Marbà, N. (2013). The role of coastal plant communities for climate change mitigation and adaptation. *Nature Climate Change*, *3*(11), 961–968. https://doi.org/10.1038/nclimate1970
Forster, P., Storelvmo, T., Armour, K., Collins, W., Dufresne, J.-L., Frame, D., Lunt, D. J., Mauritsen, T., Palmer, M. D., Watanabe, M., Wild, M., & Zhang, H. (2021). The Earth's energy budget, climate feedbacks, and climate sensitivity. In V. Masson-Delmotte, P. Zhai, A. Pirani, S. L. Connors, C. Péan, S. Berger, N. Caud, Y. Chen, L. Goldfarb, M. I. Gomis, M. Huang, K. Leitzell, E. Lonnoy, J. B. R. Matthews, T. K. Maycock, T. Waterfield, O. Yelekçi, R. Yu, & B. Zhou (Eds.), *Climate change 2021: The physical science basis. Contribution of working group I to the sixth assessment report of the intergovernmental panel on climate change* (Vol. *17*, pp. 923–1054). Cambridge University Press. https://doi.org/10.1017/9781009157896.009
Fraser, A. M., & Swinney, H. L. (1986). Independent coordinates for strange attractors from mutual information. *Physical Review A*, *33*(2), 1134–1140.
Galand, P. E., Fritze, H., & Yrjälä, K. (2003). Microsite-dependent changes in methanogenic populations in a boreal oligotrophic fen. *Environmental Microbiology*, *5*(11), 1133–1143. https://doi.org/10.1046/j.1462-2920.2003.00520.x
Galloway, J. N., Aber, J. D., Erisman, J. W., Seitzinger, S. P., Howarth, R. W., Cowling, E. B., & Cosby, B. J. (2003). The nitrogen cascade. *Bioscience*, *53*(4), 341–356. https://doi.org/10.1641/0006-3568(2003)053[0341:TNC]2.0.CO;2

Garnet, K. N., Megonigal, J. P., Litchfield, C., & Taylor, G. E. (2005). Physiological control of leaf methane emission from wetland plants. *Aquatic Botany*, *81*(2), 141–155. https://doi.org/10.1016/j.aquabot.2004.10.003

U.S. Geological Survey. (2023). *USGS 11180770 MT EDEN CR NR UNION CITY CA, in USGS water data for the Nation: U.S. Geological Survey National Water Information System database*. https://nwis.waterdata.usgs.gov/nwis/uv?site_no=11180770 [Site information directly https://waterdata.usgs.gov/nwis/dv?referred_module=sw&site_no=11180770].

Hastie, T., & Tibshirani, R. (1990). *Generalized additive models*. Chapman & Hall CRC Press.

Hill, A. C., & Vargas, R. (2022). Methane and carbon dioxide fluxes in a temperate tidal salt Marsh: Comparisons between plot and ecosystem measurements. *Journal of Geophysical Research: Biogeosciences*, *127*(7), e2022JG006943. https://doi.org/10.1029/2022JG006943

Hollinger, D. Y., & Richardson, A. D. (2005). Uncertainty in eddy covariance measurements and its application to physiological models. *Tree Physiology*, *25*(7), 873–885. https://doi.org/10.1093/treephys/25.7.873

Holmquist, J. R., & Windham-Myers, L. (2022). A conterminous USA-scale map of relative tidal Marsh elevation. *Estuaries and Coasts*, *45*(November 2021), 1596–1614. https://doi.org/10.1007/s12237-021-01027-9

Hothorn, T., Hornik, K., & Zeileis, A. (2006). Unbiased recursive partitioning: A conditional inference framework. *Journal of Computational and Graphical Statistics*, *15*(3), 651–674. https://doi.org/10.1198/106186006X133933

Hothorn, T., & Zeileis, A. (2015). Partykit: A modular toolkit for recursive Partytioning in R. *Journal of Machine Learning Research*, *16*, 3905–3909.

IPCC. (2014). *2013 supplement to the 2006 IPCC guidelines for national greenhouse gas inventories: Wetlands* [T. Hiraishi, T. Krug, T. Kiyoto, N. Srivastava, B. Jamsranjav, M. Fukuda, & T. Troxler (Eds.)]. IPCC, Switzerland. www.ipcc-nggip.iges.or.jp

Kelley, C. A., Martens, C. S., & Ussler, W. (1995). Methane dynamics across a tidally flooded riverbank margin. *Limnology and Oceanography*, *40*(6), 1112–1129. https://doi.org/10.4319/lo.1995.40.6.1112

Kirwan, M. L., Langley, J. A., Guntenspergen, G. R., & Megonigal, J. P. (2013). The impact of sea-level rise on organic matter decay rates in Chesapeake Bay brackish tidal marshes. *Biogeosciences*, *10*(3), 1869–1876. https://doi.org/10.5194/bg-10-1869-2013

Knox, S. H., Bansal, S., McNicol, G., Schafer, K., Sturtevant, C., Ueyama, M., Valach, A. C., Baldocchi, D., Delwiche, K., Desai, A. R., Euskirchen, E., Liu, J., Lohila, A., Malhotra, A., Melling, L., Riley, W., Runkle, B. R. K., Turner, J., Vargas, R., … Jackson, R. B. (2021). Identifying dominant environmental predictors of freshwater wetland methane fluxes across diurnal to seasonal time scales. *Global Change Biology*, *27*(15), 3582–3604. https://doi.org/10.1111/gcb.15661

Knox, S. H., Jackson, R. B., Poulter, B., McNicol, G., Fluet-Chouinard, E., Zhang, Z., Hugelius, G., Bousquet, P., Canadell, J. G., Saunois, M., Papale, D., Chu, H., Keenan, T. F., Baldocchi, D., Torn, M. S., Mammarella, I., Trotta, C., Aurela, M., Bohrer, G., … Zona, D. (2019). FluXNET-CH4 synthesis activity objectives, observations, and future directions. *Bulletin of the American Meteorological Society*, *100*(12), 2607–2632. https://doi.org/10.1175/BAMS-D-18-0268.1

Koenker, R. (2005). *Quantile Regression*. Cambridge University Press. https://doi.org/10.1017/CBO9780511754098

Koenker, R. (2023). *Package 'quantreg': Quantile Regression* (5.86).

Krauss, K. W., Holm, G. O., Perez, B. C., McWhorter, D. E., Cormier, N., Moss, R. F., Johnson, D. J., Neubauer, S. C., & Raynie, R. C. (2016). Component greenhouse gas fluxes and radiative balance from two deltaic marshes in Louisiana: Pairing chamber techniques and eddy covariance. *Journal of Geophysical Research: Biogeosciences*, *121*(6), 1503–1521. https://doi.org/10.1002/2015JG003224

Kroeger, K. D., Crooks, S., Moseman-Valtierra, S., & Tang, J. (2017). Restoring tides to reduce methane emissions in impounded wetlands: A new and potent blue carbon climate change intervention. *Scientific Reports*, *7*(1), 11914. https://doi.org/10.1038/s41598-017-12138-4

Kuhn, M. (2008). Building predictive models in R using the caret package. *Journal of Statistical Software*, *28*(5), 1–26. https://doi.org/10.18637/jss.v028.i05

Liu, J., Valach, A., Baldocchi, D., & Lai, D. Y. F. (2022). Biophysical controls of ecosystem-scale methane fluxes from a subtropical estuarine mangrove: multiscale, nonlinearity, asynchrony and causality. *Global Biogeochemical Cycles*, *36*, e2021GB007179. https://doi.org/10.1029/2021GB007179

Magenheimer, A. J. F., Moore, T. R., Chmura, G. L., & Daoust, R. J. (1996). Methane and carbon dioxide flux from a macrotidal salt Marsh, bay of Fundy, New Brunswick. *Estuaries*, *19*(1), 139–145. https://www.jstor.org/stable/1352658

Martens, C. S., & Berner, R. A. (1974). Methane production in the interstitial waters of sulfate-depleted marine sediments. *Science*, *185*(4157), 1167–1169. https://doi.org/10.1126/science.185.4157.1167

Martin, R. M., & Moseman-Valtierra, S. (2015). Greenhouse gas fluxes vary between Phragmites Australis and native vegetation zones in coastal wetlands along a salinity gradient. *Wetlands*, *35*(6), 1021–1031. https://doi.org/10.1007/s13157-015-0690-y

Megonigal, J. P., Hines, M. E., & Visscher, P. T. (2004). Anaerobic metabolism: Linkages to trace gases and aerobic processes. In W. H. Schlesinger, H. D. Holland, & K. K. Turekian (Eds.), *Treatise on geochemistry* (Vol. *8*, pp. 317–424). Pergamon. https://doi.org/10.1016/B978-0-08-095975-7.00808-1

Megonigal, J. P., & Schlesinger, W. H. (2002). Methane-limited methanotrophy in tidal freshwater swamps. *Global Biogeochemical Cycles*, *16*(4), 35-1–35-10. https://doi.org/10.1029/2001gb001594

Morin, T. H., Bohrer, G., Naor-Azrieli, L., Mesi, S., Kenny, W. T., Mitsch, W. J., & Schäfer, K. V. R. (2014). The seasonal and diurnal dynamics of methane flux at a created urban wetland. *Ecological Engineering*, *72*, 74–83. https://doi.org/10.1016/j.ecoleng.2014.02.002

Morris, J. T., Sundareshwar, P. V., Nietch, C. T., Kjerfve, B., & Cahoon, D. R. (2002). Responses of coastal wetlands to rising sea level. *Ecology*, *83*(10), 2869–2877. https://doi.org/10.1890/0012-9658(2002)083[2869:ROCWTR]2.0.CO;2

Mueller, P., Hager, R. N., Meschter, J. E., Mozdzer, T. J., Langley, J. A., Jensen, K., & Megonigal, J. P. (2016). Complex invader-ecosystem interactions and seasonality mediate the impact of non-native Phragmites on CH4 emissions. *Biological Invasions*, *18*(9), 2635–2647. https://doi.org/10.1007/s10530-016-1093-6

Mueller, P., Mozdzer, T. J., Langley, J. A., Aoki, L. R., Noyce, G. L., & Megonigal, J. P. (2020). Plant species determine tidal wetland methane response to sea level rise. *Nature Communications*, *11*(1), 1–9. https://doi.org/10.1038/s41467-020-18763-4

Neubauer, S. C. (2013). Ecosystem responses of a tidal freshwater Marsh experiencing saltwater intrusion and altered hydrology. *Estuaries and Coasts*, *36*(3), 491–507. https://doi.org/10.1007/s12237-011-9455-x

Neubauer, S. C., & Megonigal, J. P. (2015). Moving beyond global warming potentials to quantify the climatic role of ecosystems. *Ecosystems*, *18*(6), 1000–1013. https://doi.org/10.1007/s10021-015-9879-4

Neubauer, S. C., Miller, W. D., & Anderson, I. C. (2000). Carbon cycling in a tidal freshwater marsh ecosystem: A carbon gas flux study. *Marine Ecology Progress Series*, *199*, 13–30. https://doi.org/10.3354/meps199013

NOAA. (2023). NOAA National Estuarine Research Reserve System (NERRS). *System-wide Monitoring Program*. Data accessed from the NOAA NERRS Centralized Data Management. https://www.nerrsdata.org/

Odum, E. P. (2002). Tidal marshes as Outwelling/pulsing systems. In *Concepts and controversies in tidal Marsh ecology* (pp. 3–7). Kluwer Academic Publishers. https://doi.org/10.1007/0-306-47534-0_1

Oremland, R. S., Marsh, L. M., & Polcin, S. (1982). Methane production and simultaneous sulphate reduction in anoxic, salt marsh sediments. *Nature*, *296*(March), 143–145.

Pardo, L. H., Fenn, M. E., Goodale, C. L., Geiser, L. H., Driscoll, C. T., Allen, E. B., Baron, J. S., Bobbink, R., Bowman, W. D., Clark, C. M., Emmett, B., Gilliam, F. S., Greaver, T. L., Hall, S. J., Lilleskov, E. A., Liu, L., Lynch, J. A., Nadelhoffer, K. J., Perakis, S. S., … Dennis, R. L. (2011). Effects of nitrogen deposition and empirical nitrogen critical loads for ecoregions of the United States. *Ecological Applications*, *21*(8), 3049–3082. https://doi.org/10.1890/10-2341.1

Podgrajsek, E., Sahlée, E., Bastviken, D., Holst, J., Lindroth, A., Tranvik, L., & Rutgersson, A. (2014). Comparison of floating chamber and eddy covariance measurements of lake greenhouse gas fluxes. *Biogeosciences*, *11*(15), 4225–4233. https://doi.org/10.5194/bg-11-4225-2014

Poffenbarger, H. J., Needelman, B. A., & Megonigal, J. P. (2011). Salinity influence on methane emissions from tidal marshes. *Wetlands*, *31*(5), 831–842. https://doi.org/10.1007/s13157-011-0197-0

Reid, M. C., Tripathee, R., Schäfer, K. V. R., & Jaffé, P. R. (2013). Tidal marsh methane dynamics: Difference in seasonal lags in emissions driven by storage in vegetated versus unvegetated sediments. *Journal of Geophysical Research: Biogeosciences*, *118*(4), 1802–1813. https://doi.org/10.1002/2013JG002438

Rolston, D. E. (1986). Gas flux. In A. Klute (Ed.), *Methods of soil analysis* (pp. 1103–1119). American Society of Agronomy, Inc. and Soil Science Society of America, Inc. https://doi.org/10.2136/sssabookser5.1.2ed.c47

Rosentreter, J. A., Al-Haj, A. N., Fulweiler, R. W., & Williamson, P. (2021). Methane and nitrous oxide emissions complicate coastal blue carbon assessments. *Global Biogeochemical Cycles*, *35*(2), 1–8. https://doi.org/10.1029/2020GB006858

Rosentreter, J. A., Borges, A. V., Deemer, B. R., Holgerson, M. A., Liu, S., Song, C., Melack, J., Raymond, P. A., Duarte, C. M., Allen, G. H., Olefeldt, D., Poulter, B., Battin, T. I., & Eyre, B. D. (2021). Half of global methane emissions come from highly variable aquatic ecosystem sources. *Nature Geoscience*, *14*(4), 225–230. https://doi.org/10.1038/s41561-021-00715-2

Rosentreter, J. A., Laruelle, G. G., Bange, H. W., Bianchi, T. S., Busecke, J. J. M., Cai, W. J., Eyre, B. D., Forbrich, I., Kwon, E. Y., Maavara, T., Moosdorf, N., Najjar, R. G., Sarma, V. V. S. S., Van Dam, B., & Regnier, P. (2023). Coastal vegetation and estuaries are collectively a greenhouse gas sink. *Nature Climate Change*, *13*(6), 579–587. https://doi.org/10.1038/s41558-023-01682-9

Rosentreter, J. A., Maher, D. T., Erler, D. V., Murray, R. H., & Eyre, B. D. (2018). Methane emissions partially offset "blue carbon" burial in mangroves. *Science Advances*, *4*, eaao4985.

Roth, F., Sun, X., Geibel, M. C., Prytherch, J., Brüchert, V., Bonaglia, S., Broman, E., Nascimento, F., Norkko, A., & Humborg, C. (2022). High spatiotemporal variability of methane concentrations challenges estimates of emissions across vegetated coastal ecosystems. *Global Change Biology*, *28*(14), 4308–4322. https://doi.org/10.1111/gcb.16177

Ruddell, B. L., Brunsell, N. A., & Stoy, P. (2013). Applying information theory in the geosciences to quantify process uncertainty, feedback, scale. *Eos*, *94*(5), 56. https://doi.org/10.1002/qj.123

Ruddell, B. L., Sturtevant, C., Kang, M., & Yu, R. (2008). *ProcessNetwork software* (Version 1.5). https://github.com/ProcessNetwork/ProcessNetwork_Software

Sanders-Demott, R., Eagle, M. J., Kroeger, K. D., Wang, F., Brooks, T. W., Keefe, J. A. O., Nick, S. K., Mann, A. G., & Tang, J. (2022). Impoundment increases methane emissions in invaded coastal wetlands. *Global Change Biology*, *28*, 4539–4557. https://doi.org/10.1111/gcb.16217

Saunois, M., Stavert, A. R., Poulter, B., Bousquet, P., Canadell, J. G., Jackson, R. B., Raymond, P. A., Dlugokencky, E. J., & Houweling, S. (2020). The Global Methane Budget 2000–2017. *Earth System Science Data*, *12*, 1561–1623. https://doi.org/10.5194/essd-12-1561-2020

Schultz, M. A., Janousek, C. N., Brophy, L. S., Schmitt, J., & Bridgham, S. D. (2023). How management interacts with environmental drivers to control greenhouse gas fluxes from Pacific northwest coastal wetlands. *Biogeochemistry*, *0123456789*, 165–190. https://doi.org/10.1007/s10533-023-01071-6

Segarra, K. E. A., Samarkin, V., King, E., Meile, C., & Joye, S. B. (2013). Seasonal variations of methane fluxes from an unvegetated tidal freshwater mudflat (Hammersmith Creek, GA). *Biogeochemistry*, *115*(1–3), 349–361. https://doi.org/10.1007/s10533-013-9840-6

Seyfferth, A. L., Bothfeld, F., Vargas, R., Stuckey, J. W., Wang, J., Kearns, K., Michael, H. A., Guimond, J., Yu, X., & Sparks, D. L. (2020). Spatial and temporal heterogeneity of geochemical controls on carbon cycling in a tidal salt marsh. *Geochimica et Cosmochimica Acta*, *282*, 1–18. https://doi.org/10.1016/j.gca.2020.05.013

Sturtevant, C., Ruddell, B. L., Knox, S. H., Verfaillie, J., Matthes, J. H., Oikawa, P. Y., & Baldocchi, D. (2016). Identifying scale-emergent, nonlinear, asynchronous processes of wetland methane exchange. *Journal of Geophysical Research: Biogeosciences*, *121*(1), 188–204. https://doi.org/10.1002/2015JG003054

Tong, C., Huang, J. F., Hu, Z. Q., & Jin, Y. F. (2013). Diurnal variations of carbon dioxide, methane, and nitrous oxide vertical fluxes in a subtropical estuarine Marsh on neap and spring tide days. *Estuaries and Coasts*, *36*(3), 633–642. https://doi.org/10.1007/s12237-013-9596-1

Tong, C., Morris, J. T., Huang, J., Xu, H., & Wan, S. (2018). Changes in pore-water chemistry and methane emission following the invasion of Spartina alterniflora into an oliogohaline marsh. *Limnology and Oceanography*, *63*(1), 384–396. https://doi.org/10.1002/lno.10637

Tong, C., Wang, W., Zeng, C., & Marrs, R. (2010). Methane (CH4) emission from a tidal marsh in the Min River estuary, southeast China. *Journal of Environmental Science and Health, Part A*, *45*(4), 506–516. https://doi.org/10.1080/10934520903542261

Trifunovic, B., Vázquez-Lule, A., Capooci, M., Seyfferth, A. L., Moffat, C., & Vargas, R. (2020). Carbon dioxide and methane emissions from temperate salt Marsh Tidal Creek. *Journal of Geophysical Research: Biogeosciences*, *125*(8), e2019JG005558. https://doi.org/10.1029/2019JG005558

Turetsky, M. R., Kotowska, A., Bubier, J., Dise, N. B., Crill, P., Hornibrook, E. R. C., Minkkinen, K., Moore, T. R., Myers-Smith, I. H., Nykänen, H., Olefeldt, D., Rinne, J., Saarnio, S., Shurpali, N., Tuittila, E. S., Waddington, J. M., White, J. R., Wickland, K. P., & Wilmking, M. (2014). A synthesis of methane emissions from 71 northern, temperate, and subtropical wetlands. *Global Change Biology*, *20*(7), 2183–2197. https://doi.org/10.1111/gcb.12580

Valiela, I., & Teal, J. M. (1974). Nutrient limitation in salt masrh vegetation. In R. J. Reimold & W. H. Queen (Eds.), *Ecology of halophytes (issue 2955)*. Academic Press. https://doi.org/10.1016/b978-0-12-586450-3.50025-1

van den Berg, M., van den Elzen, E., Ingwersen, J., & Kosten, S. (2020). Contribution of plant - induced pressurized flow to CH 4 emission from a Phragmites fen. *Scientific Reports*, *10*, 12304. https://doi.org/10.1038/s41598-020-69034-7

Van der Nat, F.-J. W. A., & Middelburg, J. J. (1998). Effects of two common macrophytes on methane dynamics in freshwater sediments. *Biogeochemistry*, *43*(1), 79–104. https://doi.org/10.1023/A:1006076527187

Vargas, R., Baldocchi, D. D., Allen, M. F., Bahn, M., Black, T. A., Collins, S. L., Yuste, J. C., Hirano, T., Jassal, R. S., Pumpanen, J., & Tang, J.

(2010). Looking deeper into the soil: Biophysical controls and seasonal lags of soil CO2 production and efflux. *Ecological Applications*, *20*(6), 1569–1582. https://doi.org/10.1890/09-0693.1

Vargas, R., & Le, V. H. (2023). The paradox of assessing greenhouse gases from soils for nature-based solutions. *Biogeosciences*, *20*(1), 15–26. https://doi.org/10.5194/bg-20-15-2023

Vázquez-Lule, A., & Vargas, R. (2021). Biophysical drivers of net ecosystem and methane exchange across phenological phases in a tidal salt marsh. *Agricultural and Forest Meteorology*, *300*(June 2020), 108309. https://doi.org/10.1016/j.agrformet.2020.108309

Vroom, R. J. E., van den Berg, M., Pangala, S. R., van der Scheer, O. E., & Sorrell, B. K. (2022). Physiological processes affecting methane transport by wetland vegetation – A review. *Aquatic Botany*, *182*, 103547. https://doi.org/10.1016/j.aquabot.2022.103547

Watson, E. B., & Byrne, R. (2009). Abundance and diversity of tidal marsh plants along the salinity gradient of the San Francisco estuary: Implications for global change ecology. *Plant Ecology*, *205*(1), 113–128. https://doi.org/10.1007/s11258-009-9602-7

Weston, N. B., Neubauer, S. C., Velinsky, D. J., & Vile, M. A. (2014). Net ecosystem carbon exchange and the greenhouse gas balance of tidal marshes along an estuarine salinity gradient. *Biogeochemistry*, *120*(1–3), 163–189. https://doi.org/10.1007/s10533-014-9989-7

Wilson, B. J., Mortazavi, B., & Kiene, R. P. (2015). Spatial and temporal variability in carbon dioxide and methane exchange at three coastal marshes along a salinity gradient in a northern Gulf of Mexico estuary. *Biogeochemistry*, *123*(3), 329–347. https://doi.org/10.1007/s10533-015-0085-4

Windham-Myers, L., Cai, W.-J., Alin, S. R., Andersson, A., Crosswell, J., Dunton, K. H., Hernandez-Ayon, J. M., Herrmann, M., Hinson, A. L., Hopkinson, C. S., Howard, J., Hu, X., Knox, S. H., Kroeger, K., Lagomasino, D., Megonigal, J. P., Najjar, R. G., Paulsen, M.-L., Peteet, D., … Watson, E. B. (2018). Chapter 15: Tidal wetlands and estuaries. In N. Cavallaro, G. Shrestha, R. Birdsey, M. A. Mayes, R. G. Najjar, S. C. Re, P. RomeroLankao, & Z. Zhu (Eds.), *Second state of the carbon cycle report (SOCCR2): A sustained assessment report (pp. 596–648)*. U.S. Global Change Research Program. https://doi.org/10.7930/SOCCR2.2018.Ch15

Wood, S. N. (2011). Fast stable restricted maximum likelihood and marginal likelihood estimation of semiparametric generalized linear models. *Journal of the Royal Statistical Society (B)*, *73*(1), 3–36. https://doi.org/10.1111/j.1467-9868.2010.00749.x

Yu, K., Hiscox, A., & DeLaune, R. D. (2013). Greenhouse gas emission by static chamber and eddy flux methods. In R. D. DeLaune, K. R. Reddy, C. J. Richardson, & J. P. Megonigal (Eds.), *Methods in Biogeochemistry of wetlands (issue 10, pp. 427–437)*. Soil Science Society of America. https://doi.org/10.2136/sssabookser10.c22

Yuan, K., Li, F., McNicol, G., Chen, M., Hoyt, A., Knox, S., Riley, W. J., Jackson, R., & Zhu, Q. (2024). Boreal-Arctic wetland methane emissions modulated by warming and vegetation activity. *Nature Climate Change*, *14*(3), 282–288. https://doi.org/10.1038/s41558-024-01933-3

Zhang, Z., Poulter, B., Feldman, A. F., Ying, Q., Ciais, P., Peng, S., & Li, X. (2023). Recent intensification of wetland methane feedback. *Nature Climate Change*, *13*(5), 430–433. https://doi.org/10.1038/s41558-023-01629-0

## SUPPORTING INFORMATION

Additional supporting information can be found online in the Supporting Information section at the end of this article.

**How to cite this article:** Arias-Ortiz, A., Wolfe, J., Bridgham, S. D., Knox, S., McNicol, G., Needelman, B. A., Shahan, J., Stuart-Haëntjens, E. J., Windham-Myers, L., Oikawa, P. Y., Baldocchi, D. D., Caplan, J. S., Capooci, M., Czapla, K. M., Derby, R. K., Diefenderfer, H. L., Forbrich, I., Groseclose, G., Keller, J. K., … Holmquist, J. R. (2024). Methane fluxes in tidal marshes of the conterminous United States. *Global Change Biology*, *30*, e17462. https://doi.org/10.1111/gcb.17462